Implications of a Changing Arctic on Summertime Rates of Air-Sea CO_2 Exchange within the Eastern Canadian Arctic

by

Tonya Burgers

A Thesis submitted to the Faculty of Graduate Studies of

The University of Manitoba

In partial fulfillment of the requirements of the degree of

MASTER OF SCIENCE

Department of Environment and Geography

University of Manitoba

Winnipeg

ABSTRACT

The Arctic marine system is currently undergoing transition as a result of climate change. This study examines the effects of this transition on rates of air-sea CO_2 exchange within the eastern Canadian Arctic. Continuous seawater pCO_2 measurements revealed this area to be a strong summertime sink of atmospheric CO_2. Total alkalinity and stable oxygen isotopes were utilized as freshwater tracers, revealing areas of significant sea ice melt and riverine inputs. Eastern Baffin Bay and Barrow Strait were found to be strongly influenced by sea ice melt, lowering seawater pCO_2; whereas Kennedy Channel contained significant river discharge, raising seawater pCO_2. Primary production in surface waters was low throughout the region, with the exception of Petermann Fjord where glacial ice melt likely transports nutrients to the surface. This region is anticipated to represent a weaker CO_2 sink in the future, due mainly to predicted decreases in sea ice thickness and extent.

ACKNOWLEDGEMENTS

Foremost I wish to sincerely thank my advisor Dr. Tim Papakyriakou for his never-ending patience, support, and encouragement, as well as my committee members Drs. Jens Ehn and Brian Amiro for their insight and suggestions. I also wish to thank Drs. Lisa Miller, Helmuth Thomas, Michel Gosselin, Yves Gratton, and Alfonso Mucci for being so willing to share their unique datasets with me, and Drs. Kumiko Azetsu-Scott and Robie Macdonald for their enthusiasm in sharing their expertise.

I extend a special thank you to Brent Else and Meredith Pind for teaching me the ropes on my very first Arctic field expedition, and to Sebastian Luque and Emmelia Wiley for their assistance in field-prep, lab work, and data processing. I am also very thankful to the captain and crew of CCGS Amundsen for their tireless efforts in ensuring all scientists onboard accomplish their goals.

This study would not have been possible without the financial support of ArcticNet, a Network of Centre's of Excellence of Canada, the Natural Science and Engineering Research Council (NSERC), and personal support from the Northern Scientific Training Program (NSTP).

Last but certainly not least, thank you to my friends and family for your encouragement throughout this endeavor. Especially thank you to Josh, who is a constant source of fun and inspiration.

DEDICATION

To my good friend Kristen Leal, thank you for pushing me out of my comfort zone - all the way to the North Pole.

TABLE OF CONTENTS

Abstract ii

Acknowledgements iii

Dedication iv

List of Figures vi

List of Tables viii

List of Copyrighted Material viii

1.0 Introduction 1

1.1 Research Objectives 2

1.2 Thesis Outline 2

2.0 Literature Review 3

2.1 Air-Sea Exchange of CO_2 3

2.2 Seawater Carbonate Chemistry 6

1.1.1 Processes affecting pCO_{2sw} 8

2.3 Freshwater Tracers 14

2.3.1 Stable Oxygen Isotopes 14

2.3.2 Total Alkalinity 19

2.4 The Baffin Bay Marine System 21

2.4.1 Circulation and Water Masses 22

2.4.2 Freshwater Inputs 25

2.4.3 The North Water Polynya 26

3.0 Data and Methods 28

3.1 Surface Water pCO_2 Sampling 28

3.2 Atmospheric Measurements 29

3.3 Sea Ice Observations 30

3.4 Air-Sea CO_2 Flux Calculations 30

3.5 Ancillary Measurements 31

3.5.1 Carbonate System 33

3.5.2 Oxygen Isotopes 33

3.5.3 Chlorophyll-a 34

3.6 Freshwater Decomposition 34

3.7 Temperature Normalization 37

4.0 Results 39

4.1 Parameters at the Sea Surface 39

4.2 Rates of Air-Sea CO_2 Exchange 44

4.3 Processes controlling the distribution of pCO_{2sw} 46

4.3.1 Water Masses 46

4.3.2 Temperature Variations 48

4.3.3 Freshwater Inputs 50

4.3.4 Primary Productivity 56

5.0 Discussion 58

5.1 Influence of the Arctic Oscillation 58

5.2 The Role of Glacial Ice Melt 59

5.3 Future Implications of Increased Freshwater 61

6.0 Conclusions 63

References 67

LIST OF FIGURES

Figure 1: Six commonly employed parameterizations of the transfer velocity (k) where U_{10} is the wind speed at a height of 10 m and k_{660} is the transfer velocity computed at a Schmidt number of 660 (representative of seawater at 25 °C). WM99 refers to Wanninkhof and McGillis (1999), W92 refers to Wanninkhof (1992), S07 refers to Sweeney et al. (2007), H06 refers to Ho et al. (2006), W14 refers to Wanninkhof (2014), and N00 refers to Nightingale et al. (2000). 5

Figure 2: Schematic illustration of the seawater carbonate system (Zeebe and Wolf-Gladrow, 2001) © 2015 Elsevier. 7

Figure 3: Effect of various processes on DIC and TA indicated by arrows. Solid and dashed lines indicate constant concentrations of dissolved CO_2 and pH respectively (Zeebe and Wolf-Gladrow, 2001) © 2015 Elsevier 13

Figure 4: The global distribution of $\delta^{18}O$ in precipitation based on 389 WMO GNIP (Global Networks for Isotopes in Precipitation) stations between 1961 and 1999 (McGuire and McDonnell, 2007) © 2015 Blackwell Publishing. 17

Figure 5: Schematic indicating approximate salinity/ $\delta^{18}O$ values and mixing relationships between sea ice melt (SIM), meteoric water (MW), and seawater within the Arctic Ocean. 19

Figure 6: Schematic indicating approximate salinity/TA values and mixing relationships between sea ice melt (SIM), river runoff (RW), and seawater within the Arctic Ocean. 20

Figure 7: Bathymetry of Baffin Bay, with depth contours at 500, 1000, and 2000 m. Red letters on map indicate locations of: B – Barrow Strait, C – Clyde River, D – Disko Island, DI – Devon Island, DS – Davis Strait, H – Hell's Gate, J – Jones Sound, K – Kane Basin, L – Lancaster Sound, M – Melville Bay, N – Nares Strait, R – Robeson Channel, S – Smith Sound, Y – Cape York (Tang et al., 2004) © 2015 Elsevier. 22

Figure 8: Schematic of surface circulation within the Canadian Arctic Archipelago and Baffin Bay. Larger arrows point to the Arctic Circumpolar Boundary Current, which continues along the North American continental shelf as the dashed line, as well as the strong southward current within Nares Strait. (McLaughlin et al., 2004) © 2006 by the President and Fellows of Harvard University. 23

Figure 9: Geographical location and average May extent of the North Water Polynya. © 2015 The PEW Charitable Trusts. 27

Figure 10: Sampling locations for ancillary measurements of $\delta^{18}O$ (upright triangle), TA/DIC (inverted triangle), and Chlorophyll-*a* (cross). 32

Figure 11: Continuous underway pCO_{2sw} measurements collected in summer 2013 and 2014. 39

Figure 12: Underway measurements of surface seawater temperature (T_{sw}) and salinity collected during summer of 2013 and 2014. 41

Figure 13: pCO_{2sw} measurements from 2013 (left column) and 2014 (right column) presented in temperature-salinity space in Baffin Bay (a,b), Lancaster Sound and Barrow Strait (c,d), the NOW polynya region (e,f), and Nares Strait (g,h). Circled areas represent regions of freshwater inputs and/or upwelling contributing to significant fluctuations in pCO_{2sw}. Axes have been scaled to show trends. 43

Figure 14: Calculated rates of air-sea CO_2 exchange within the eastern Canadian Arctic. Negative values denote oceanic uptake of atmospheric CO_2. 45

Figure 15: Variations in $npCO_{2sw}$ (temperature-normalized pCO_{2sw}) throughout the eastern Canadian Arctic during summer of 2013 and 2014. 49

Figure 16: Calculated surface freshwater fractions based on $\delta^{18}O$ (2013) and TA (2014) samples collected at discrete sampling stations (indicated by black dots). 51

Figure 17: Fractions of sea ice melt (F_{sim}) throughout the surface mixed layer of eastern Baffin Bay. The inset map shows the locations of sampling stations in this area. Inset plots show salinity and TA measurements used in the calculation of freshwater fractions. 52

Figure 18: Fractions of river runoff (Frr) within Nares Strait, the four most northerly stations in this transect represent Kennedy Channel. The inset map shows station locations in this area. Inset plots show salinity and TA measurements used in the calculation of freshwater fractions. 54

Figure 19: Subsurface chlorophyll-a maximum (SCM) located in the northeastern NOW polynya region in 2013. Inset map shows sampling station locations in this area. 57

LIST OF TABLES

Table 1: Endmember definitions for 2013 freshwater decomposition. 37

Table 2: End-member definitions for 2014 freshwater decomposition. 37

LIST OF COPYRIGHTED MATERIAL

Figure 2: Schematic illustration of the seawater carbonate system (Zeebe and Wolf-Gladrow, 2001) © 2015 Elsevier. 7

Figure 3: Effect of various processes on DIC and TA indicated by arrows. Solid and dashed lines indicate constant concentrations of dissolved CO_2 and pH respectively (Zeebe and Wolf-Gladrow, 2001) © 2015 Elsevier 13

Figure 4: The global distribution of $\delta^{18}O$ in precipitation based on 389 WMO GNIP (Global Networks for Isotopes in Precipitation) stations between 1961 and 1999 (McGuire and McDonnell, 2007) © 2015 Blackwell Publishing. 17

Figure 7: Bathymetry of Baffin Bay, with depth contours at 500, 1000, and 2000 m. Red letters on map indicate locations of: B – Barrow Strait, C – Clyde River, D – Disko Island, DI – Devon Island, DS – Davis Strait, H – Hell's Gate, J – Jones Sound, K – Kane Basin, L – Lancaster Sound, M – Melville Bay, N – Nares Strait, R – Robeson Channel, S – Smith Sound, Y – Cape York (Tang et al., 2004) © 2015 Elsevier. ... 22

Figure 8: Schematic of surface circulation within the Canadian Arctic Archipelago and Baffin Bay. Larger arrows point to the Arctic Circumpolar Boundary Current, which continues along the North American continental shelf as the dashed line, as well as the strong southward current within Nares Strait. (McLaughlin et al., 2004) © 2006 by the President and Fellows of Harvard University. 23

Figure 9: Geographical location and average May extent of the North Water Polynya. © 2015 The PEW Charitable Trusts. 27

1.0 INTRODUCTION

Since the advent of the industrial revolution anthropogenic activities have brought about steep increases in atmospheric CO_2 concentrations. It has long been known that significant increases of greenhouse gases (such as CO_2) would raise surface air temperatures by trapping more radiative energy within the Earth's atmosphere [*Arrhenius*, 1896]. The ongoing accumulation of atmospheric CO_2 continues to be the largest driver of contemporary climate change. However, the global oceans represent a significant sink of atmospheric CO_2, absorbing roughly one quarter of anthropogenic emissions released every year [*Le Quéré et al.*, 2010]. Polar oceans such as the Arctic Ocean have been found to represent an enhanced CO_2 sink in comparison to other world oceans, due to its relatively high biological productivity and low surface water temperatures [*Bates and Mathis*, 2009].

The Arctic region however, is undergoing some of the most intense and severe climate change on the planet. Surface air temperatures within the Arctic have increased at double the rate of the global average [*Serreze and Barry*, 2011] and in recent years the sea ice cover of the Arctic Ocean has severely diminished [*Stroeve et al.*, 2007]. It has been predicted that the Arctic Ocean may be fully ice-free throughout the summer season as early as 2020 [*Overland and Wang*, 2013]. Further evidence of warming in the Arctic arises from observations of increased glacial ice melt and riverine inputs to the surface ocean [*Déry et al.*, 2009; *Rignot et al.*, 2011]. Drastic changes such as these will have knock-on effects within the Arctic ecosystem, and affect changes in the carbonate chemistry of Arctic waters. It remains unclear whether the net effect of these changes will reduce or enhance the CO_2 uptake capacity of the Arctic Ocean.

1.1 Research Objectives

The overall purpose of this study is to determine how current climate change is affecting rates of air-sea CO_2 exchange throughout the eastern Canadian Arctic; defined here as the region including northern Baffin Bay, and the eastern channels of the CAA including Nares Strait. This region has not received much attention in recent years in terms of its seawater carbonate chemistry. Specifically, we will investigate the impacts of changes in water mass distributions, biological production, freshwater inputs, and sea surface temperatures throughout the region. The two main objectives of this investigation are:

1) To determine the strength of air-sea CO_2 fluxes throughout the region, and whether summertime exchange rates represent an overall source or sink of atmospheric CO_2.
2) To determine the regionally specific controls affecting variations in surface seawater pCO_2, as this parameter determines the magnitude of air-sea CO_2 fluxes.

1.2 Thesis Outline

This thesis is composed of six chapters. The first chapter introduces the rationale and outline of this thesis. The second chapter provides a comprehensive review of the literature supporting this analysis, with subsections discussing factors known to influence rates of air-sea CO_2 exchange and seawater carbonate chemistry, chemical tracers of freshwater, and a review of the oceanographic setting of the eastern Canadian Arctic. Chapter three provides a description of the data and methods utilized in this investigation. Chapter four presents the results of this investigation, with chapter five providing a discussion of these results. Finally, chapter six provides an overview of the conclusions of this study and presents recommendations for future research.

2.0 LITERATURE REVIEW

This literature review is intended to provide a comprehensive overview of the theory and past scientific studies upon which this work is based. Section 2.1 discusses the estimation of air-sea CO_2 fluxes using measurements of sea surface and atmospheric pCO_2. Section 2.2 provides a detailed review of seawater carbonate chemistry, and the many processes known to influence seawater pCO_2. Section 2.3 discusses the application of chemical tracers in identifying freshwater inputs throughout the surface oceans, and finally section 2.4 will provide an introduction to the oceanography of the Baffin Bay region.

2.1 AIR-SEA EXCHANGE OF CO_2

Air-sea fluxes of CO_2 are commonly estimated using the bulk parameterization:

$$F_{CO_2} = \alpha k(pCO_{2sw} - pCO_{2atm}) \quad (1)$$

where F_{CO_2} represents the flux of CO_2, α is the solubility of CO_2 in seawater, k is the transfer velocity, and pCO_{2sw} and pCO_{2atm} represent the partial pressure of CO_2 within the surface seawater and atmosphere respectively [*Wanninkhof et al.*, 2009]. This equation consists of two main components: (1) the pCO_2 gradient, which determines both the potential for, and the direction of the air-sea CO_2 flux, and (2) the transfer velocity, k, which determines the rate at which the flux can occur. The bulk flux equation is set up to conform with the common convention that a negative CO_2 flux represents a sink of CO_2, and a positive flux represents a source of CO_2 to the atmosphere. Essentially, if pCO_{2sw} is lower than pCO_{2atm}, the ocean will act as a CO_2 sink; however if pCO_{2sw} is greater than pCO_{2atm} the ocean will outgas CO_2 to the atmosphere. Generally, since the value of pCO_{2atm} does not change over short timescales, changes in pCO_{2sw} will ultimately determine whether a certain region of the ocean will act as a

source or sink of CO_2. Several physical and biogeochemical processes affect the value of pCO_{2sw} within the surface seawater, which are discussed in greater detail in section 2.2.1.

The magnitude of the transfer velocity (k) is determined as a function of water-side turbulence, as increased amounts of turbulence within the ocean's surface layer lead to enhanced air-sea exchange. Although multiple factors influence water-side turbulence, k is commonly parameterized solely as a function of wind speed and temperature. This is the case as wind velocity is an easily measured variable, and has a strong influence on surface turbulence. Many studies have been conducted using wind tunnels [*Liss and Merlivat*, 1986], natural and/or deliberate tracers [*Wanninkhof*, 1992, 2014; *Nightingale et al.*, 2000; *Ho et al.*, 2006; *Sweeney et al.*, 2007], or other micrometeorological techniques [*Wanninkhof and McGillis*, 1999] to derive parameterizations of transfer velocity under different wind and temperature conditions. Figure 1 shows a number of common parameterizations of transfer velocity as functions of wind speed measured from a height of 10 metres (U_{10m}), and the Schmidt number (*Sc*). The Schmidt number is defined as the ratio of the kinematic viscosity of water divided by the mass diffusion coefficient of the gas in question [*MacIntyre et al.*, 1995], in this case CO_2. The dependence of k on sea surface temperature is expressed through *Sc*.

Figure 1 demonstrates that there is a great deal of scatter among the parameterizations for transfer velocity, especially at high wind speeds. This scatter is representative of the large uncertainty that still exists within parameterizations of k, and may also indicate that wind speed and temperature alone are not the only factors controlling k. Many other factors are known to

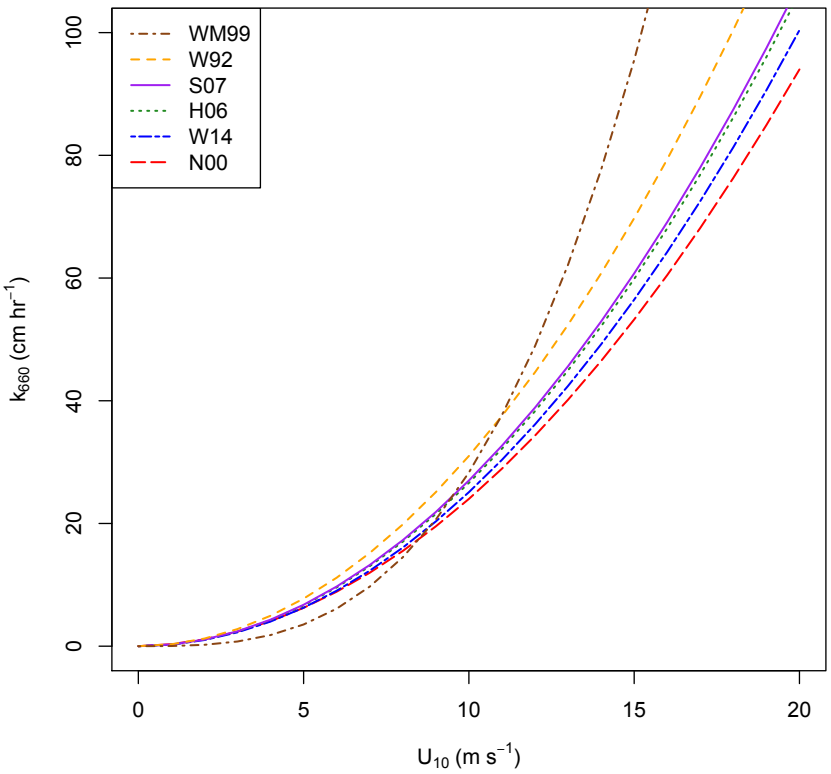

Figure 1: Six commonly employed parameterizations of the transfer velocity (k) where U_{10} is the wind speed at a height of 10 m and k_{660} is the transfer velocity computed at a Schmidt number of 660 (representative of seawater at 25 °C). WM99 refers to Wanninkhof and McGillis (1999), W92 refers to Wanninkhof (1992), S07 refers to Sweeney et al. (2007), H06 refers to Ho et al. (2006), W14 refers to Wanninkhof (2014), and N00 refers to Nightingale et al. (2000).

influence water-side turbulence, such as increased wave state [*Zappa et al.*, 2004], fetch [*Woolf*, 2005], buoyancy [*McGillis et al.*, 2004], tides [*Zappa et al.*, 2007], rain [*Zappa et al.*, 2009], ocean currents [*MacIntyre et al.*, 1995], and the presence of surface films [*Frew*, 1997; 2004]. Additionally, the majority of field studies conducted to create these parameterizations have been located in low and mid-latitude oceans, or in some cases freshwater lakes [*Liss and Merlivat*, 1986], with only one study being conducted at high-latitudes in the Southern Ocean [*Ho et al.*, 2006]. Therefore, parameterizations of *k* are also influenced by various location-dependent factors, further contributing to the scatter seen in Figure 1. General circulation models currently

make use of these parameterizations, along with sea-surface observations of pCO_{2sw}, in order to estimate global rates of air-sea CO_2 exchange.

2.2 Seawater Carbonate Chemistry

To comprehend the many biogeochemical processes impacting rates of air-sea CO_2 exchange, an understanding of the seawater carbonate system is required. Carbon dioxide does not simply dissolve in water like other gases such as nitrogen and oxygen; instead CO_2 subsequently reacts with water and is partitioned among four different chemical species: aqueous carbon dioxide [$CO_{2\ (aq)}$], carbonic acid [H_2CO_3], bicarbonate [HCO_3^-], and carbonate [CO_3^{2-}]. These four chemical species are all related by the following equilibria, making up the seawater carbonate system:

$$CO_{2\ (aq)} + H_2O \leftrightarrow H_2CO_3 \leftrightarrow HCO_3^- + H^+ \leftrightarrow CO_3^{2-} + 2H^+ \quad (2)$$

The concentration of H_2CO_3 is much smaller than that of $CO_{2\ (aq)}$, and these two neutrally charged species are not chemically separable. Therefore, the sum of these two species is commonly denoted as CO_2, or $H_2CO_3^*$ in the literature [*Zeebe and Wolf-Gladrow*, 2001]. Herein we will use the former notation:

$$CO_2 = CO_{2\ (aq)} + H_2CO_3 \quad (3)$$

Using this notation, the carbonate system simplifies to the series of equilibrium reactions shown in Figure 2, where both the initial exchange of CO_2 between the atmosphere and ocean, and the subsequent equilibria of dissolved CO_2 are illustrated.

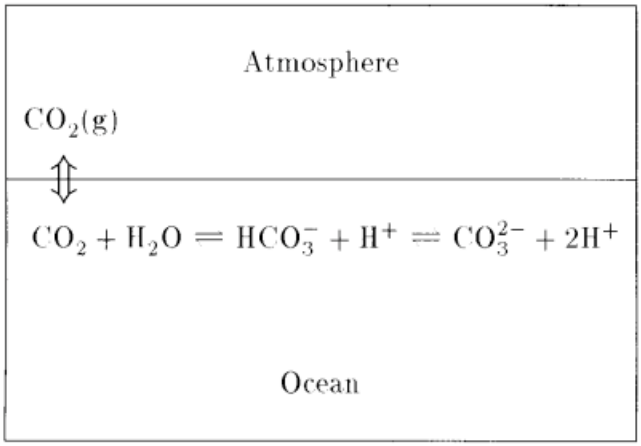

Figure 2: Schematic illustration of the seawater carbonate system (Zeebe and Wolf-Gladrow, 2001) © 2015 Elsevier.

The air-sea exchange of CO_2 can be described by the equilibrium reaction:

$$CO_{2\,(g)} \overset{K_0}{\leftrightarrow} CO_2 \tag{4}$$

where the concentration of dissolved CO_2 is given by Henry's Law, with the equilibrium constant K_0 being the solubility coefficient of CO_2 in seawater [*Zeebe and Wolf-Gladrow*, 2001]. The seawater carbonate equilibria is represented as:

$$CO_2 + H_2O \overset{K_1}{\leftrightarrow} HCO_3^- + H^+ \overset{K_2}{\leftrightarrow} CO_3^{2-} + 2H^+ \tag{5}$$

where the equilibrium constants K_1 and K_2 are often referred to as the first and second dissociation constants of carbonic acid, respectively. All aforementioned equilibrium constants (K_0, K_1, and K_2) are dependent on the temperature and salinity of the seawater. Therefore, any changes to these physical properties of seawater will alter the equilibrium state of the carbonate system, changing the ability of the water to absorb CO_2 from the atmosphere.

In order to efficiently characterize the carbonate system of seawater, oceanographers have found it useful to define two key parameters; dissolved inorganic carbon (DIC), and total alkalinity (TA) as:

$$DIC = \Sigma CO_2 = [CO_2] + [HCO_3^-] + [CO_3^{2-}] \quad (6)$$

$$TA = [HCO_3^-] + 2[CO_3^{2-}] + [B(OH)_4^-] + [OH^-] - [H^+] + \ minor\ components \quad (7)$$

DIC is simply the sum of all inorganic carbon species present in seawater, while TA is a measure of the excess of bases (or proton acceptors) over acids (or proton donors). While DIC keeps track of the inorganic carbon dissolved in seawater, TA keeps track of the charges. Both of these parameters strongly influence the carbonate chemistry of seawater, and thus control the amount of CO_2 that can be dissolved. For instance, if DIC is increased (decreased), the dissolved concentration of CO_2 will also increase (decrease). On the other hand, if TA is increased (decreased), the dissolved concentration of CO_2 will decrease (increase). Figure 3 illustrates how DIC and TA affect the dissolved concentration of CO_2 and seawater pH. Measurements of DIC, TA and the temperature and salinity of seawater allows for the complete characterization of the carbonate system [*Zeebe and Wolf-Gladrow*, 2001]. Therefore, many processes that affect the seawater carbonate system (and the amount of dissolved CO_2) are best described in terms of their associated changes in DIC and TA.

1.1.1 Processes affecting pCO_{2sw}

Thus far it has been determined that any processes affecting the equilibrium constants or the DIC/TA of seawater will affect the amount of CO_2 that can be absorbed from the atmosphere. The following section reviews several physical and biological processes that influence seawater carbonate chemistry, and hence pCO_{2sw}.

1.1.1.1 Physical Processes

Two aforementioned processes that affect the seawater carbonate system are temperature and salinity. Since cold water can dissolve more CO_2 than warm water, an increase in temperature will increase pCO_{2sw} [*Weiss*, 1974]. Similarly, an increase in seawater salinity will also act to increase pCO_{2sw}. Takahashi et al. (1993) tested the dependency of pCO_{2sw} on temperature by holding DIC and TA constant in a seawater sample while altering the temperature of the sample. The results of this study provided a very useful equation for characterizing changes in pCO_{2sw} with temperature:

$$\frac{\partial \ln pCO_{2sw}}{\partial T} \approx 0.0423°C^{-1} \tag{8}$$

Similarly, the dependence of pCO_{2sw} on seawater salinity (while holding DIC and TA constant) can be characterized as [*Sarmiento and Gruber*, 2006]:

$$\frac{\partial \ln pCO_{2sw}}{\partial \ln S} \approx 1 \tag{9}$$

Within the global oceans surface seawater temperature varies by about 30°C, whereas salinity varies only by about 7 psu. Therefore, temperature should be regarded as the larger physical control over pCO_{2sw} [*Sarmiento and Gruber*, 2006]. Furthermore, changes in seawater salinity are mainly driven by the processes of evaporation and precipitation (or in the case of the Arctic Ocean, sea ice melt and river runoff), which would not only modify the salinity of the seawater, but also DIC and TA. For example, increasing salinity through evaporation would act to concentrate DIC and TA, while decreasing salinity through precipitation would dilute DIC and TA. These corresponding changes in DIC/TA with changing salinity act to enhance the salinity dependence of pCO_{2sw} by approximately 60% [*Sarmiento and Gruber*, 2006]. This means that

the addition of freshwater may decrease pCO_{2sw} more significantly than expected from equation (9), while the removal of freshwater (without removing DIC/TA) would increase pCO_{2sw}.

The impact of various sources of freshwater is of particular interest to this study, as the Arctic Ocean is strongly influenced by riverine inputs, sea ice melt, and glacial ice melt. The Arctic Ocean receives 11% of Earth's river runoff, despite only accounting for 1% of global ocean seawater [*Shiklomanov*, 2000]. Thus the Arctic Ocean is disproportionally impacted by riverine inputs, particularly in coastal regions and on the continental shelves. Biological processes and the dissolution of carbonate minerals occur throughout the length of a river, contributing to enriched DIC and TA in river runoff that enters the Arctic Ocean. Rivers are generally heterotrophic environments (respiration dominates over photosynthesis), therefore contributing greatly to DIC; conversely, sea ice melt is generally depleted in DIC and TA. During sea ice formation TA and DIC become concentrated within the brine channels of the sea ice, and subsequently expelled from the sea ice matrix back into the water column [*Anderson et al.*, 2004; *Rysgaard et al.*, 2007; *Miller et al.*, 2011]. These dense brines sink within the water column, carrying TA and DIC to deeper waters where they may be sequestered for long periods of time. When temperatures increase in spring and sea ice begins to melt, very little TA or DIC remains within the ice; thus the resulting meltwater plume is depleted in these two parameters. Few studies have investigated the TA and DIC of glacial ice within the Arctic; however, of those that have been conducted glacial meltwater has exhibited extremely low TA and DIC, contributing to low pCO_{2sw} at the surface [*Sejr et al.*, 2011; *Rysgaard et al.*, 2012; *Evans et al.*, 2014].

The final physical process that affects pCO_{2sw} directly is air-sea gas exchange. As mentioned in section 2.1, the amount of CO_2 being transferred across the ocean-atmosphere interface is

determined by two key variables: (1) the transfer velocity (determined as a function of wind speed), and (2) the pCO_2 gradient between the atmosphere and ocean. The process of air-sea gas exchange is constantly acting to bring both the pCO_2 of the atmosphere and surface ocean into equilibrium; however this is rarely achieved because of the equilibrium reactions of carbonate species within seawater. For every 20 dissolved CO_2 molecules, approximately 19 of them will react with carbonate (the strongest base of the carbonate system) to form bicarbonate molecules, leaving only one molecule remaining as dissolved CO_2 [*Sarmiento and Gruber*, 2006]. Because of the equilibrium reactions governing the concentrations of carbonate species, the timescale for ocean-atmosphere equilibration of pCO_2 via gas transfer is estimated on the scale of months. Most other processes that have been previously described act on much shorter timescales, and therefore air-sea gas exchange is not as important in determining pCO_{2sw} as most other modifying processes.

1.1.1.2 Biological Processes

Biological processes are also capable of altering the carbonate chemistry of seawater. Photosynthesis and the reverse reaction of remineralization are perhaps the most obvious of these processes. Photosynthesis is the main mechanism through which pCO_{2sw} is lowered in surface seawater. Phytoplankton convert CO_2, nutrients, and water into organic matter through the following equation [*Redfield et al.*, 1963]:

$$CO_{2(aq)} + NO_{3(aq)}^{-} + HPO_{4(aq)}^{2-} + H_2O_{(l)} + H_{(aq)}^{+} \leftrightarrow C_{106}H_{175}O_{42}N_{16}P + O_{2(g)} \quad (10)$$

From this equation it is evident that the process of photosynthesis will reduce pCO_{2sw} by directly consuming $CO_{2\,(aq),}$ but also by consuming $H^{+}_{(aq)}$ which will lower TA and further decrease pCO_{2sw}. The process of photosynthesis is limited by the availability of light and nutrients.

Examples of nutrients are the chemical species NO_3^- (nitrate) and HPO_4^{2-} (phosphate) within equation (10), and no organic material can be formed in the absence of these compounds. Large phytoplankton blooms often deplete nutrients within the surface layer if there are no other external sources to replenish the local supply. A major source of nutrients is the deep ocean, and therefore productivity tends to be higher in regions of upwelling.

Remineralization (also called respiration) is essentially the reverse reaction of photosynthesis, and it will therefore have the effect of decreasing pCO_{2sw}. During this process heterotrophic organisms (e.g. zooplankton) consume organic material and return organic carbon and inorganic nitrogen to their inorganic states. This process can occur both within the surface layer and the deep ocean, as heterotrophic organisms do not require light. Therefore, any organic matter that sinks to the deep ocean may later be remineralized, causing deep waters to be enriched in nutrients and DIC.

A third biological process of importance in carbon cycling is the biogenic formation and dissolution of calcium carbonates. Some phytoplankton (e.g. coccolithophores) and zooplankton (e.g. foraminifera) form calcite or aragonite shells through the reaction:

$$Ca^{2+} + CO_3^{2-} \leftrightarrow CaCO_3 \tag{11}$$

This reaction influences pCO_{2sw} as the consumption of CO_3^{2-} lowers DIC and decreases TA twofold (since carbonate has a charge of 2-). Therefore the net effect of creating (dissolving) calcium carbonate is to slightly increase (decrease) pCO_{2sw}. Organisms that form calcium carbonate shells generally sink to greater depths when they die, creating a net export of DIC and TA from the surface to the deep ocean [*Sarmiento and Gruber*, 2006].

Figure 3 summarizes the resultant changes to TA, DIC, [CO_2] (the molar concentration of dissolved CO_2, in μmol kg^{-1}) and pH for each of the physical and biological processes previously mentioned, and visually demonstrates how changes in TA and DIC affect the dissolved concentration of CO_2. For example, the process of air-sea CO_2 exchange only results in changes to DIC and not TA, as it adds/subtracts carbonate species from the water without affecting its overall charge. Conversely, photosynthesis (respiration) moderately affects TA, as charged chemical species are being taken up (released) by organisms that create (consume) organic matter. Similarly, the formation/dissolution of calcium carbonate affects the charge balance (and hence TA) of the surrounding seawater as carbonate ions (CO_3^{2-}) are consumed/released. These carbonate ions also affect DIC as they contribute to the overall sum of inorganic carbon species within the water.

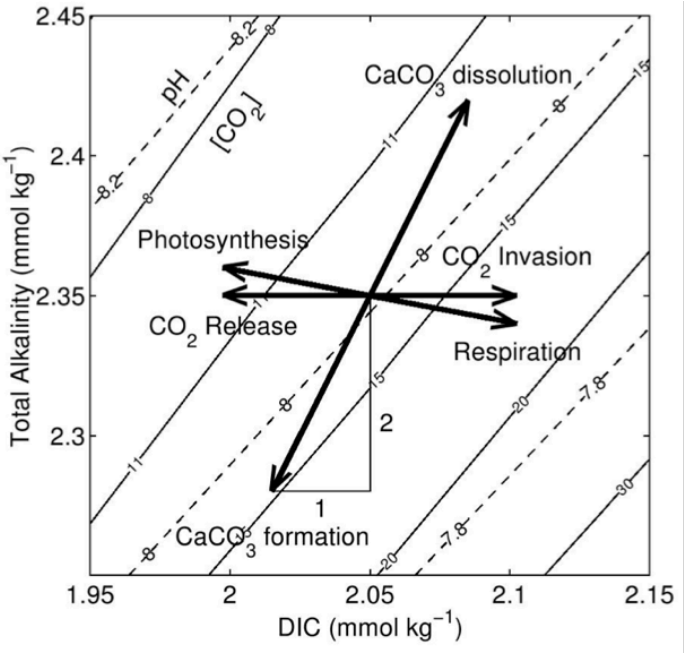

Figure 3: Effect of various processes on DIC and TA indicated by arrows. Solid and dashed lines indicate constant concentrations of dissolved CO_2 and pH respectively (Zeebe and Wolf-Gladrow, 2001) © 2015 Elsevier

2.3 Freshwater Tracers

This section discusses the use of certain chemical constituents within seawater to identify the distribution and abundance of freshwater sources. Many studies have been conducted using stable oxygen isotopes to distinguish sea ice meltwater from continental runoff and precipitation [*Tan and Strain*, 1980; *Bédard et al.*, 1981; *Östlund and Hut*, 1984; *Macdonald et al.*, 1995]. More recently Yamamoto-Kawai et al. [2005] demonstrated that alkalinity (TA) is another tracer that can be used within the Arctic Ocean to distinguish between these freshwater sources.

2.3.1 Stable Oxygen Isotopes

Isotopes are defined as atoms having the same number of protons, but different numbers of neutrons within the atomic nucleus. The term *isotopes* is derived from Greek meaning equal places - as isotopes share the same position on the periodic table. Standard notation for isotopes is ${}^{A}_{Z}E$ where E is the element, A is the atomic mass (the combined mass of protons and neutrons in the nucleus), and Z is the number of protons. Often the subscript Z is omitted, as isotopes of the same element will have the same number of protons. There are three stable oxygen isotopes: ^{16}O, ^{17}O, and ^{18}O, which have global abundances of 99.7628%, 0.0372% and 0.20004% respectively [*Zeebe and Wolf-Gladrow*, 2001]. The ratio of ^{18}O to ^{16}O is usually reported because of the higher abundance of ^{18}O compared to ^{17}O.

Due to the difference in mass between isotopes they will exhibit some differing physiochemical properties. For example, as water molecules transition from one phase to another there is some partitioning of isotopes between phases; this partitioning is termed isotopic fractionation. Two different types of isotopic fractionation exist: equilibrium and kinetic. Equilibrium fractionation

involves the partitioning of isotopes between phases or compounds of a system that is in equilibrium. In terms of a chemical reaction, this means that isotopic fractionation can occur even when there is no net reaction occurring. On the other hand, kinetic fractionation occurs when there is a net forward reaction, but the reaction rates differ between molecules containing the light and heavy isotope [*Zeebe and Wolf-Gladrow*, 2001]. Within the global hydrological cycle, the process of evaporation represents an example of kinetic fractionation. During evaporation lighter ^{16}O isotopes are preferentially taken into the vapour phase as they require less energy input to make this transition, leaving the remaining liquid water enriched with heavier ^{18}O isotopes. Fractionation during evaporation has been shown to decrease with increasing temperature [*Majoube*, 1971]. Additional isotopic fractionation occurs during the process of precipitation. Here the heavier molecules condense first, and therefore precipitation is enriched in ^{18}O. This is termed the Rayleigh distillation process, and causes the remaining water vapour in clouds to become further depleted in ^{18}O as more water droplets condense. This fractionation is also temperature-dependent, with greater fractionation occurring at lower temperatures [*Zeebe and Wolf-Gladrow*, 2001].

When comparing the ratios of oxygen isotopes $\left(\frac{^{18}O}{^{16}O}\right)$ scientists use a standard called V-SMOW (Vienna Standard Mean Ocean Water), which represents the standard isotopic composition of ocean water. Since the primary source of water for the global hydrological cycle is the ocean, the V-SMOW standard is a logical selection to compare against all other water samples. Oxygen isotope ratios that are compared against the V-SMOW standard are expressed in delta notation ($\delta^{18}O$) defined as the per mil (‰) deviation of the isotope ratio in a sample from that of the V-SMOW standard:

$$\delta^{18}O\ (‰) = \left[\frac{\left(\frac{^{18}O}{^{16}O}\right)_{sample}}{\left(\frac{^{18}O}{^{16}O}\right)_{VSMOW}} - 1\right] \times 1000 \quad (12)$$

As per this definition, the $\delta^{18}O$ value of the V-SMOW standard is 0 ‰. Deviations in seawater $\delta^{18}O$ from V-SMOW are largely controlled by isotopic fractionation associated with the processes of evaporation and precipitation. Further processes causing isotopic fractionation, such as ice formation, are discussed below. The majority of evaporation from the global oceans occurs in the tropics. During evaporation ^{16}O isotopes are preferentially converted into water vapour, creating clouds. As these clouds travel north or south of the tropics the water vapour within them condenses, forming precipitation. The earliest precipitation formed is the most enriched in ^{18}O, whereas precipitation released at higher latitudes is further depleted in ^{18}O. This creates a roughly zonal pattern of $\delta^{18}O$ variability in precipitation, depicted in Figure 4. A large majority of the precipitation that falls on land returns to the oceans via continental runoff, adding freshwater with low $\delta^{18}O$ to the surface ocean.

As shown in Figure 4, $\delta^{18}O$ values of precipitation for the Arctic region can range from -15‰ to -25‰ depending on the exact location. Glacial ice melt can be even further depleted in ^{18}O, exhibiting $\delta^{18}O$ values between -25‰ to -40‰ [*Reeh et al.*, 2002]. This occurs because the $\delta^{18}O$ values of glacial ice depend not only on latitude effects, but also the age of the ice. The isotopic composition of the oceans does not stay constant over geological timescales, and therefore the $\delta^{18}O$ of glacial ice reflects conditions of the hydrological cycle from thousands of years ago. Additionally, colder temperatures during glacial periods increase isotopic fractionation, ultimately leading to precipitation that is further depleted in ^{18}O than during interglacial periods.

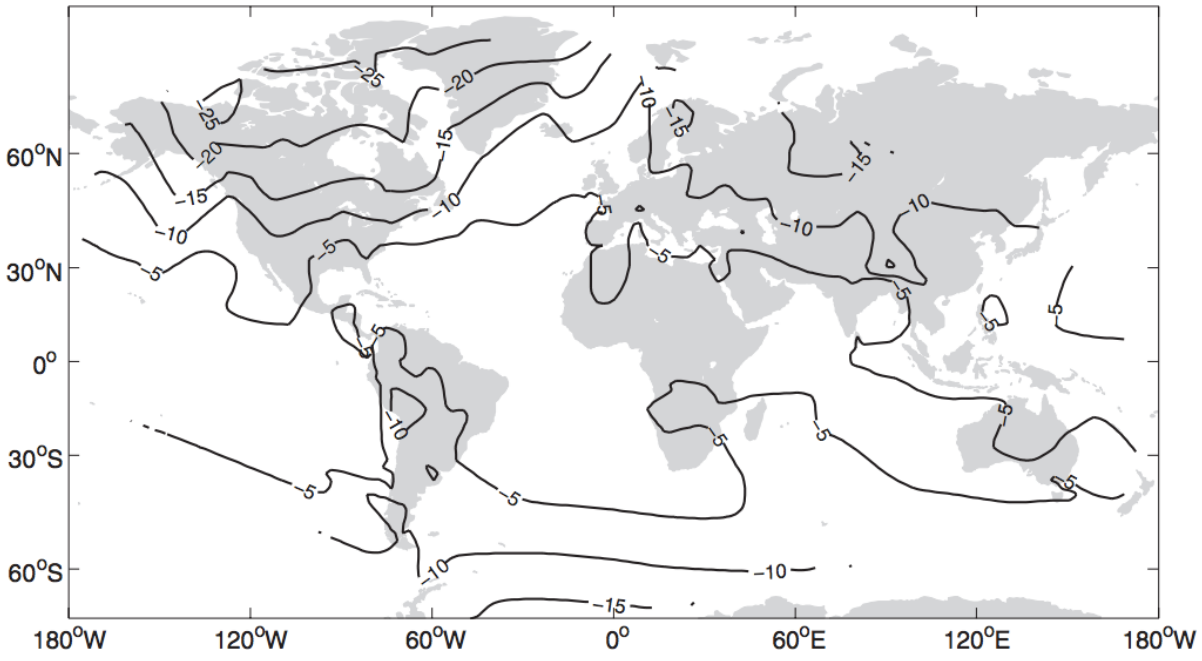

Figure 4: The global distribution of $\delta^{18}O$ in precipitation based on 389 WMO GNIP (Global Networks for Isotopes in Precipitation) stations between 1961 and 1999 (McGuire and McDonnell, 2007) © 2015 Blackwell Publishing.

2.3.1.1 Salinity- $\delta^{18}O$ relationships in the Arctic Ocean

Surface waters within the Arctic Ocean are affected by many sources of freshwater including direct precipitation, land runoff, sea ice melt, and glacial ice melt. Freshwater content in the ocean is defined relative to a reference salinity, which in the Arctic Ocean is commonly taken to be the salinity of Atlantic seawater (S ~ 34.9). Thus Pacific water represents a source of freshwater to the Arctic Ocean, as its salinity is much fresher than that of Atlantic seawater. Pacific water contains freshwater accumulated from rivers and precipitation within the Pacific Ocean and Bering Sea. Further discussion of Pacific vs. Atlantic water masses within the Arctic Ocean will be presented in section 2.4.

While all freshwater sources have low salinities, some have widely ranging $\delta^{18}O$ values, which makes it possible to differentiate their sources and quantify their proportions. As previously stated, precipitation and land runoff at high latitudes have negative values of $\delta^{18}O$, with land ice from glaciers and ice caps displaying slightly more negative values of $\delta^{18}O$. The freshwater from these three sources have all commonly undergone distillation and transport in the atmosphere before being returned to the surface ocean, and are therefore commonly referred to as "meteoric water". Conversely, sea ice meltwater displays slightly more positive $\delta^{18}O$ than that of the surface seawater from which it was formed (0‰ to low positive values). This is the result of isotopic fractionation that preferentially incorporates heavier ^{18}O isotopes into the solid state [*Macdonald et al.*, 1995]. Sea ice withdraws freshwater from the surface ocean during its formation, and adds freshwater back during melt. As these two processes are decoupled in time and space, they have the potential to affect freshwater distributions within the Arctic Ocean.

Figure 5 displays approximate end-member values of sea ice melt (SIM), meteoric water (MW), and Atlantic seawater in salinity-$\delta^{18}O$ space with mixing lines between the seawater and freshwater sources. Seawater samples that are solely affected by one freshwater source (i.e. sea ice meltwater or meteoric water) will lie along either of these mixing lines. Seawater samples that are affected by a combination of all three end-members will lie somewhere in salinity-$\delta^{18}O$ space between the mixing lines. Seawater that has been affected by brine expulsion from sea ice formation will exhibit an enhanced salinity signal, and also a more negative $\delta^{18}O$ value as ^{18}O isotopes are preferentially retained within the solid ice. Therefore in salinity- $\delta^{18}O$ space seawater samples containing brine would lie on the opposite side of the meteoric-seawater mixing line from sea ice melt.

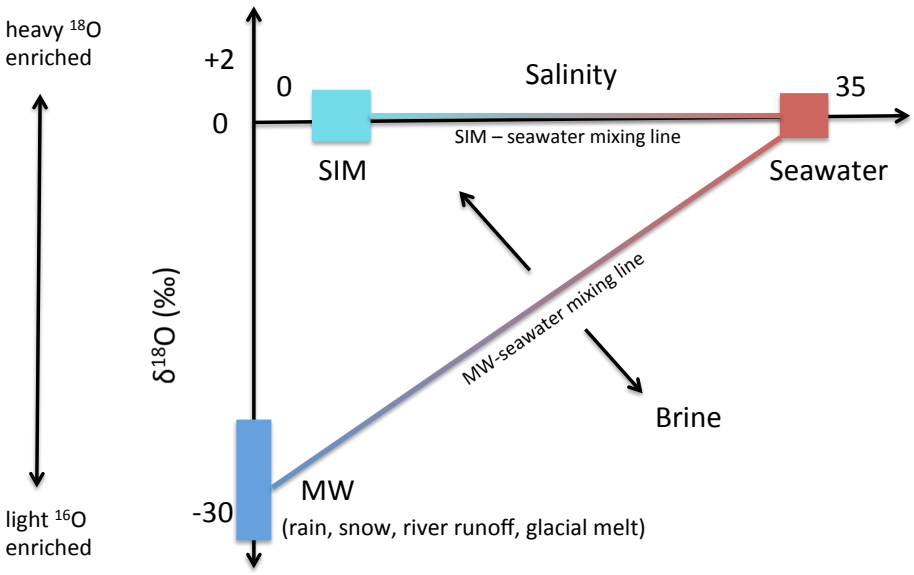

Figure 5: Schematic indicating approximate salinity/ $\delta^{18}O$ values and mixing relationships between sea ice melt (SIM), meteoric water (MW), and seawater within the Arctic Ocean.

2.3.2 Total Alkalinity

Total alkalinity (TA) is another chemical tracer that can be used to identify freshwater inputs. Similar to $\delta^{18}O$, the TA end-members of various freshwater sources are quite different. Arctic river runoff exhibits relatively high TA (~1000 µmol kg^{-1}) due to the dissolution of carbonate minerals and the decay of organic matter within the river prior to its drainage into the Arctic Ocean. Conversely, the TA of sea ice melt (< 300 µmol kg^{-1}) and direct precipitation (near zero) are very low in comparison. The TA of sea ice melt is low because most of the salts and chemical compounds that contribute to TA become concentrated into brine channels within the sea ice. The brine is later expelled into the water column, leaving the remaining sea ice depleted in TA.

Figure 6 illustrates approximate end-member values for sea ice melt (SIM), river runoff (RW), and Atlantic seawater in salinity-TA space with mixing lines between the seawater and freshwater sources. Seawater samples that are solely affected by either SIM or RW will lie along the SIM-seawater or RW-seawater mixing lines respectively. Seawater samples affected by all three end-members will lie somewhere between the mixing lines. Seawater that has been affected by brine will exhibit higher TA and salinity in comparison to SIM.

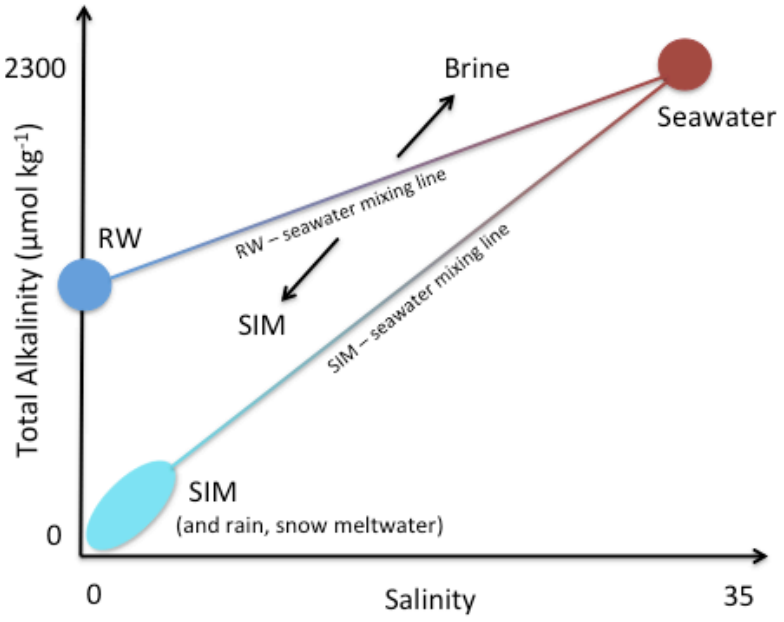

Figure 6: Schematic indicating approximate salinity/TA values and mixing relationships between sea ice melt (SIM), river runoff (RW), and seawater within the Arctic Ocean.

It is important here to note the use of river runoff and not meteoric water. River runoff and precipitation are almost identical in $\delta^{18}O$, thus they can be represented collectively as "meteoric water"; however they are largely different in TA. Meteoric water supply is thought to be dominated by river runoff in the high Arctic [*Schlosser and Newton*, 2002]. Yamamoto-Kawai et al. [2005] performed a comparison of estimated freshwater fractions using both salinity-TA and salinity- $\delta^{18}O$ relationships throughout the Arctic Ocean. They found that estimated freshwater

fractions from both tracers agreed well, and presented the same freshwater distribution trends throughout both the Eurasian and Canadian sectors of the Arctic Ocean.

2.4 The Baffin Bay Marine System

Baffin Bay is a semi-enclosed peripheral sea of the Arctic Ocean located between Baffin Island to the west and Greenland to the east that serves as a conduit for Arctic waters flowing to the North Atlantic Ocean. It therefore provides an important pathway for the exchange of heat, salt, and other chemical constituents of seawater. The location and bathymetry of Baffin Bay is depicted in Figure 7, along with the many passages of the Canadian Arctic Archipelago (CAA). Baffin Bay contains a large abyssal plain in its central region with depths in excess of 2300 m, and the continental shelf off of Baffin Island is relatively narrow in comparison to the Greenland side. On its southern end Baffin Bay is connected to the north Atlantic via Davis Strait, a 300 km wide and 1000 m deep channel [*Hamilton and Wu*, 2013]. The connection to the Arctic Ocean is far more restricted, consisting of many relatively narrow and shallow passages through the CAA. Three main channels transport the majority of Arctic waters through the CAA; Jones Sound, Lancaster Sound and Nares Strait. The most narrow of these passages is Jones Sound with a 120 m deep sill at Hell's Gate. The other shallow connection is to the west of Lancaster Sound at Barrow Strait with a sill depth of 150 m. The deepest connection is via Nares Strait, with the shallowest point located at the 250 m deep sill in Kane Basin [*Tang et al.*, 2004].

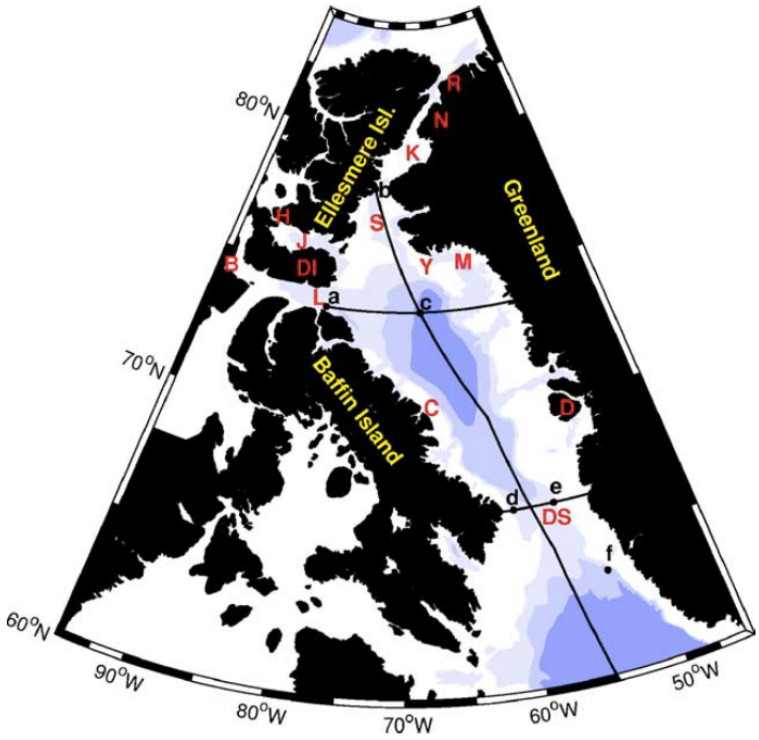

Figure 7: Bathymetry of Baffin Bay, with depth contours at 500, 1000, and 2000 m. Red letters on map indicate locations of: B – Barrow Strait, C – Clyde River, D – Disko Island, DI – Devon Island, DS – Davis Strait, H – Hell's Gate, J – Jones Sound, K – Kane Basin, L – Lancaster Sound, M – Melville Bay, N – Nares Strait, R – Robeson Channel, S – Smith Sound, Y – Cape York (Tang et al., 2004) © 2015 Elsevier.

2.4.1 Circulation and Water Masses

There is an overall cyclonic circulation of seawater within Baffin Bay comprised of two main currents, the southward flowing Baffin Island Current (BIC) and the northward flowing West Greenland Current (WGC). The shallow passages of the CAA act as an outflow shelf, transporting Arctic surface waters southwards into Baffin Bay. This Arctic outflow is transported primarily through Nares Strait, Jones Sound, and Lancaster Sound, with the flows of these three channels merging in northern Baffin Bay to form the BIC. Although the channels of the CAA support a net outflow from the Arctic Ocean, the greater widths of some channels allow for more complicated circulations, including reverse flow. McLaughlin et al. [2004] describe counter-

flows along the northern coasts of Jones and Lancaster Sounds, which are shown along with general circulation of Baffin Bay and the CAA in Figure 8.

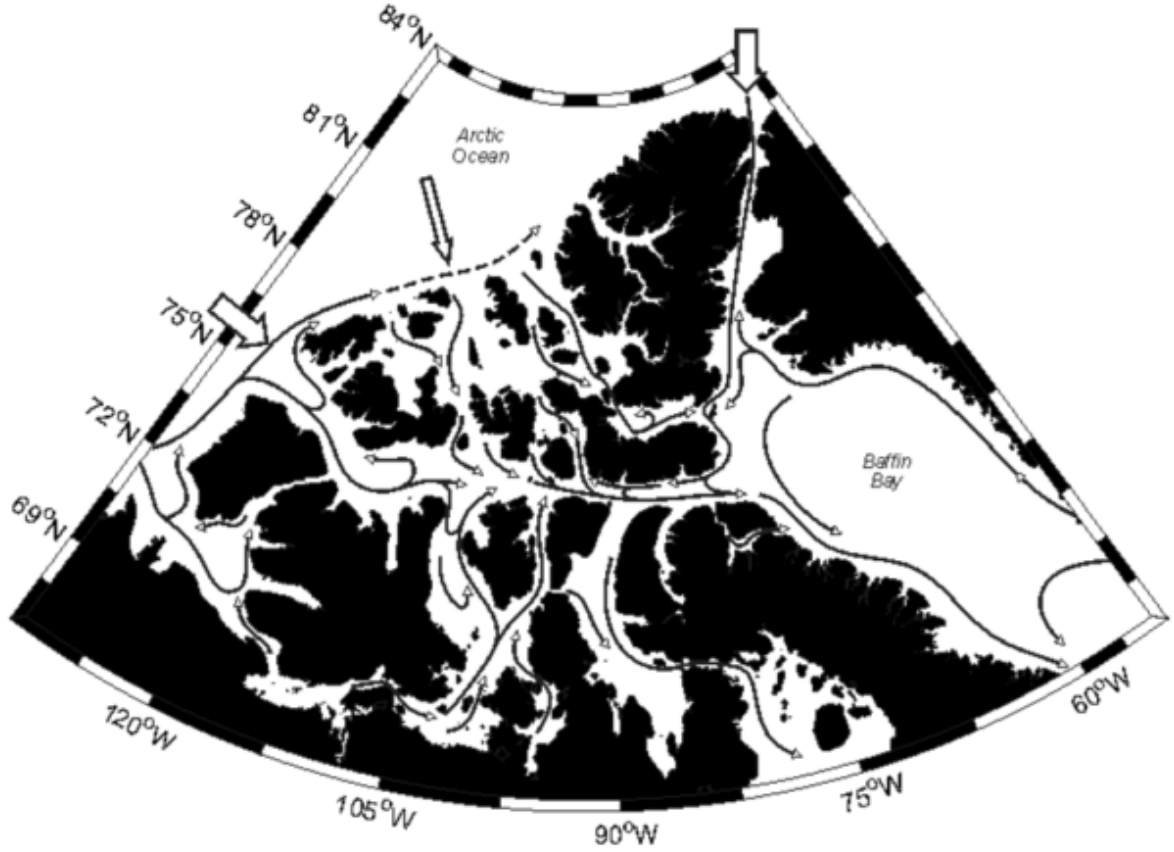

Figure 8: Schematic of surface circulation within the Canadian Arctic Archipelago and Baffin Bay. Larger arrows point to the Arctic Circumpolar Boundary Current, which continues along the North American continental shelf as the dashed line, as well as the strong southward current within Nares Strait. (McLaughlin et al., 2004) © 2006 by the President and Fellows of Harvard University.

The WGC also transports Arctic waters into Baffin Bay as a continuation of the East Greenland Current (EGC), which originates in Fram Strait (the passage between Greenland and Svalbard) and carries Arctic surface waters south along the eastern coast of Greenland. Hopkins [1991] showed that Arctic waters carried by the EGC remain geostrophically constrained to the Greenland continental margin, allowing them to steer around the southern tip of Greenland and continue northwards with the WGC. The WGC also brings warmer and more saline Atlantic

waters from the Irminger Sea as an extension of the Irminger Current [*Clarke*, 1984]. These two different water masses carried by the WGC are commonly referred to as West Greenland Shelf water (WGSW) and West Greenland Irminger Water (WGIW).

At cold temperatures the density of seawater is primarily determined by salinity, causing the Arctic Ocean and its peripheral seas to be salinity-stratified. Therefore, the relatively fresh Arctic waters are present within the surface mixed layer of Baffin Bay, with the more saline Atlantic water below. On the eastern side of Baffin Bay WGSW is generally found in the upper 100 m and is characterized by $T > 4°C$ and $S < 33.5$ whereas WGIW is present at depths between 200 and 500 m with $T > 2°C$ and $S > 34.5$. Between these two water masses is a cold halocline layer, characterized by a steep salinity gradient and temperatures near the freezing point. Generally the temperature minimum is assumed to represent the bottom of the surface layer, and the start of the halocline. The strong stratification of the halocline prevents mixing between the surface waters and the warm Atlantic waters below, ultimately preventing heat from reaching the surface. This helps to both promote winter sea ice growth and maintain sea ice cover. On the western side of Baffin Bay the surface layer is comprised of Arctic outflow from the CAA, which can extend to depths of 300 m due to the presence of the BIC. Below this is the cold halocline layer, followed by WGIW at depths between 400 to 600 m. The most dense and deep waters of Baffin Bay are aptly named Baffin Bay Deep Water (BBDW) and are present at depths greater than 600 m; these waters are characterized by $T < 2°C$ and $S > 34.5$.

2.4.2 Freshwater Inputs

Freshwater entering Baffin Bay has four main sources: river runoff, sea ice meltwater, Pacific water, and the glacial meltwater. Arctic waters transported through the CAA consist largely of Pacific waters that have travelled from the Bering Sea along the North American continent by the Arctic Circumpolar Boundary Current (shown as the dashed current in Figure 8). Portions of the Arctic Circumpolar Boundary Current branch off and enter the various passages of the CAA.

The EGC carries freshwater in both solid (sea ice) and liquid forms southwards out of the Arctic Ocean. Solid sea ice accounts for over half of the Arctic freshwater export through Fram Strait [*de Steur et al.*, 2009; *Spreen et al.*, 2009], and freshwater additions from the Greenland ice sheet and precipitation add to the freshwater content of the EGC [*Sutherland and Pickart*, 2008]. As discussed previously the EGC eventually feeds into the WGC, and so this freshwater content is transported northwards along the eastern edge of Baffin Bay.

Glacial ice melt from Greenland represents a rapidly increasing freshwater input to the north Atlantic Ocean. Bamber et al. [2010] used a regional climate model to determine that 80% of the total Greenland discharge enters the ocean on the western and south-eastern coasts, and that from 1992 to 2010 the discharge into Baffin Bay, the Labrador Sea, and the Irminger Sea has increased by 22%, 48% and 49% respectively. The glaciers and ice caps located on islands of the CAA are also contributing to increased freshwater in Baffin Bay, although they only represent 10% of the Greenland ice sheet volume [*Sharp et al.*, 2011].

2.4.3 The North Water Polynya

A polynya is defined as a persistent and recurrent area of open water and/or thin ice cover in a region that would be climatologically expected to have a solid ice cover (Smith et al., 1990). Polynyas form as a result of complex interactions between ocean thermodynamics, atmospheric circulation patterns, and sea ice conditions. The North Water (NOW) Polynya is a recurrent area of open water (or light ice conditions) located at the northern end of Baffin Bay; it represents the largest polynya in the northern hemisphere, spanning the area between northern Baffin Bay and Smith Sound (see Figure 7 for locations). Figure 9 shows both the geographical location and average extent of the NOW polynya.

The NOW polynya is classified as an ice-bridge polynya as the formation of an ice-bridge in Nares Strait is critical in its formation [*Wilson et al.*, 2001]. When the ice-bridge forms it blocks the southerly flow of sea ice through Nares Strait and into Baffin Bay. Once the ice-bridge has formed, a combination of latent and sensible heat mechanisms act to maintain the polynya. Latent heat mechanisms export sea ice from polynya regions through a combination of strong winds and surface currents, whereas sensible heat mechanisms prevent the formation of sea ice by providing heat to the surface layer [*Mundy and Barber*, 2001; *Barber and Massom*, 2007]. Latent heat mechanisms affecting the NOW polynya are the result of channeled surface winds through Nares Strait, creating strong northerly winds which export sea ice towards the south [*Ito*, 1982]. This is the main mechanism maintaining the NOW polynya, however sensible-heat mechanisms also play a small role in the formation of the eastern reaches of the polynya. The presence of the relatively warm WGC along the eastern edge of the polynya provides heat to the surface mixed layer, slowing ice growth in this area [*Mundy and Barber*, 2001].

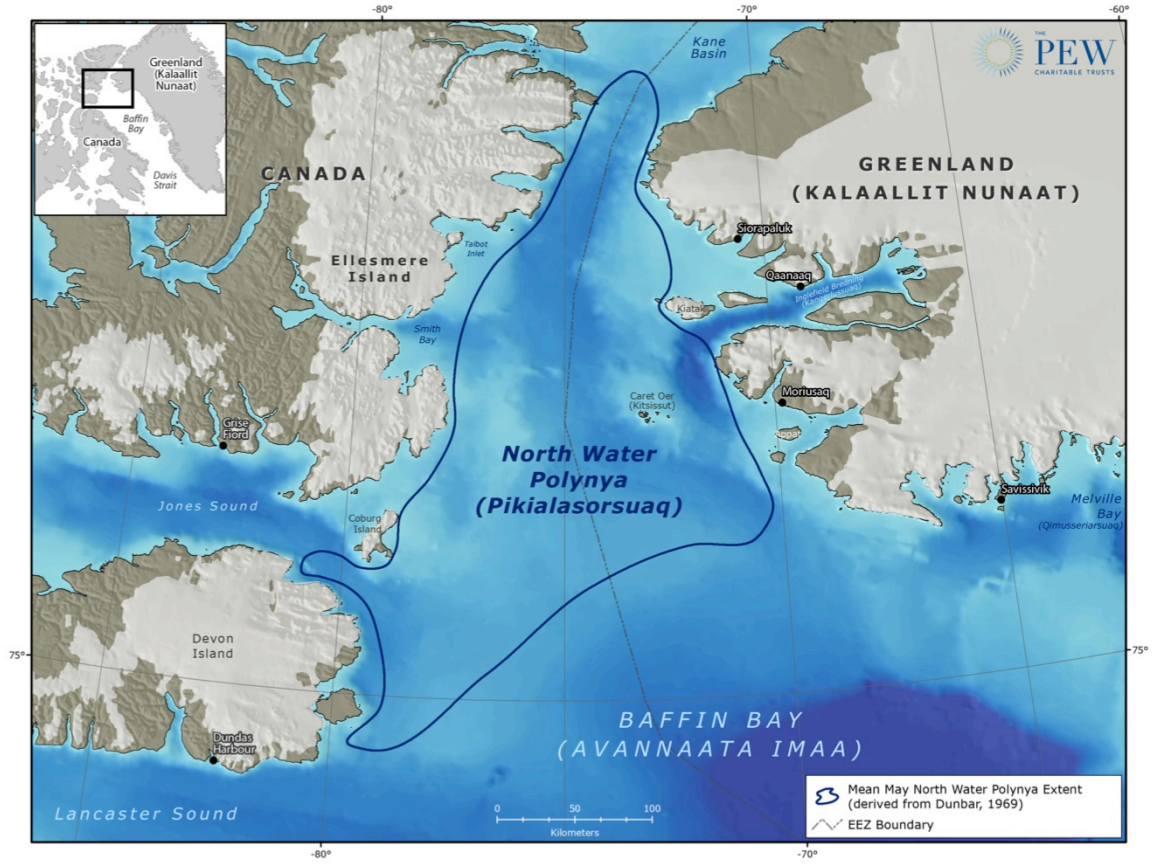

Figure 9: Geographical location and average May extent of the North Water Polynya. © 2015 The PEW Charitable Trusts.

The NOW polynya is also one of the most biologically productive areas in the Arctic Ocean. The absence of sea ice in this area contributes to an especially early spring phytoplankton bloom. Large concentrations of marine mammals such as beluga whales, walrus, seals, and polar bears have been observed feeding around the ice edge until break-up at the end of spring [*Stirling*, 1980]. It has been observed that strong northerly winds from Nares Strait contribute to the mixing of surface waters with deeper nutrient-rich waters and once these strong surface winds begin to die down in summer the productivity of these waters is greatly reduced [*Tremblay et al.*, 2002].

3.0 DATA AND METHODS

Data used in this study were collected during the 2013 and 2014 ArcticNet scientific cruises aboard CCGS Amundsen. Both cruises were conducted during the summer season, with the 2013 cruise taking place from July 25th to Sept 2nd and the 2014 cruise being conducted slightly earlier from July 8th to Aug 10th. Throughout the cruise a meteorological tower on the ship's foredeck as well as an underway system were continuously sampling atmospheric and surface seawater pCO_2, providing us with continuous measurements of the air-sea pCO_2 gradient. Ancillary measurements of DIC, TA, $\delta^{18}O$, and Chlorophyll-*a* were collected using the ship's rosette at scheduled sampling stations. However, not all ancillary measurements were collected at each station. In-situ sea ice observations were also collected hourly from the ship's bridge.

3.1 SURFACE WATER pCO_2 SAMPLING

An underway pCO_2 system (General Oceanics model 8050 [*Pierrot et al.*, 2009]), was operated throughout each cruise, continuously sampling water from a high-volume inlet located at a depth of 5 m. Water was cycled through the underway system at a rate of 2.4 – 2.8 L min^{-1}, and calibrations of the system's infrared gas analyzer (LI-COR model LI-7000) were monitored twice daily against three certified gas standards (CO_2 concentrations of 0.0, 373.07, 600.02 ppm in 2013, and 0.0, 377.90, 600.20 ppm in 2014) traceable to WMO standards. The underway system has an expected accuracy of 2 μatm [*Pierrot et al.*, 2009]. Despite close proximity to the inlet, a temperature probe in the equilibrator measured a slight increase in water temperature relative to on-station measurements made by the ship's conductivity-temperature-depth (CTD) sensor. For our 2013 measurements we corrected for the temperature increase using a regression analysis comparing equilibrator water temperatures to coincident surface water measurements

made by the ship's CTD. This comparison revealed a strong (R^2=0.98) linear relationship (T_{sw} = 1.01*T_{eq} – 0.93°C) between equilibrator water temperature (T_{eq}) and in situ surface water temperature (T_{sw}). This relationship was then used to correct pCO_2 measurements using the procedure of Takahashi et al. [1993]. For the 2014 cruise a temperature probe was installed directly into the ship's seawater intake line, and these temperature measurements were used to correct for thermodynamic effects following the same procedure. The underway system also includes a flow-through CTD (Idronaut model Ocean Seven 315) which provides coincident salinity measurements. Throughout the cruise, instances where the underway pCO_2 system was being cleaned, calibrated or sea ice blocked the intake line resulted in missing data.

3.2 Atmospheric Measurements

A meteorological tower was installed on the foredeck of the research vessel to monitor atmospheric variables relevant to air-sea gas exchange. Wind speed and direction were measured using a conventional propeller anemometer (RM Young Co. model 15106MA) located at a nominal height of 16 m above the sea surface. Atmospheric CO_2 was measured using a closed-path infrared gas analyzer (LI-COR model LI-7000) with an intake located at a height of ~13 m on the meteorological tower. Measurements from these instruments were recorded as 1 min averages on a data logger (Campbell Scientific Inc. model CR-1000). Data were discarded during instances when the meteorological tower was lowered to clean and/or calibrate the instruments, or when winds were coming from the stern of the vessel. Winds from the stern become distorted by the body of the ship, and also carry exhaust from the ship's stack towards the CO_2 sensors on the tower.

3.3 Sea Ice Observations

Sea ice observations were recorded hourly from the ship's bridge, with 24-hour observations recorded throughout the 2013 cruise, and 12-hour observations during the 2014 cruise. These observations include information on sea ice concentration (in 10ths) as well as ice type. For periods when hourly sea ice observations were not collected during the 2014 cruise, the observation log was supplemented using weekly ice charts from the Canadian Ice Service (iceweb1.cis.ec.gc.ca).

3.4 Air-Sea CO_2 Flux Calculations

Rates of air-sea CO_2 exchange were estimated using equation (1), where k (the transfer velocity) was parameterized according to Sweeney et al. (2007):

$$k = 0.27 U_{10m}^2 (Sc/660)^{-1/2} \quad (13)$$

where U_{10m} is wind speed at 10 m height, and Sc is the Schmidt number. For utilization in equation (13), wind speed measurements were corrected to a height of 10 m using the log linear profile, assuming a neutral surface layer following Stull [1988]. The Schmidt number was estimated as a function of sea surface temperature (SST) according to Jähne et al. [1987]. The Sweeney et al. (2007) k parameterization was selected as it agrees well with direct measurements of k at low to moderate wind speeds [*McGillis et al.*, 2001] and at high wind speeds [*Ho et al.*, 2006]. The parameterization is based on global inventories of ^{14}C, and is therefore less likely to be influenced by location dependent variables compared to other available parameterizations. However, because there is currently no consensus on which parameterization is best within the Arctic region, in this study we follow the approach of Else et al. [2008] in utilizing the

parameterizations of Nightingale et al. [2000] and Wanninkhof [1992] as the lower and upper bounds on *k* estimates.

Air-sea CO_2 fluxes were calculated as average exchange rates over 30 min periods, with each period requiring at least 20 wind speed and SST measurements to obtain an accurate average *k*. The solubility coefficient (α) was estimated from SST following Weiss [1974], and the pCO_2 gradient was calculated using atmospheric and surface seawater pCO_2 measurements from the meteorological tower and underway system respectively. The average pCO_{2atm} from each cruise was used in equation (1), with values of 390.1 ppm in 2013 and 387.6 ppm in 2014. Using sea ice observations collected hourly from the ship's bridge, open water fluxes were corrected for sea ice concentration by linearly scaling the flux proportionally to the fraction of open water. It is acknowledged that this approach is a crude simplification of what is likely a complicated process, however there is currently no widely accepted alternative to this approach. A number of recent studies have used the approach we adopt here [*Mucci et al.*, 2010; *Else et al.*, 2013a; *Cross et al.*, 2014].

3.5 Ancillary Measurements

At designated stations throughout the cruise seawater samples were collected for ancillary measurements of DIC, TA, $\delta^{18}O$ and Chlorophyll-*a*. However, not all ancillary measurements were conducted at every sampling station. Sampling locations for each variable are shown in Figure 10. Samples were collected from the ship's CTD/Rosette system, which consists of 24 12L Niskin bottles and a CTD (SeaBird 911+).

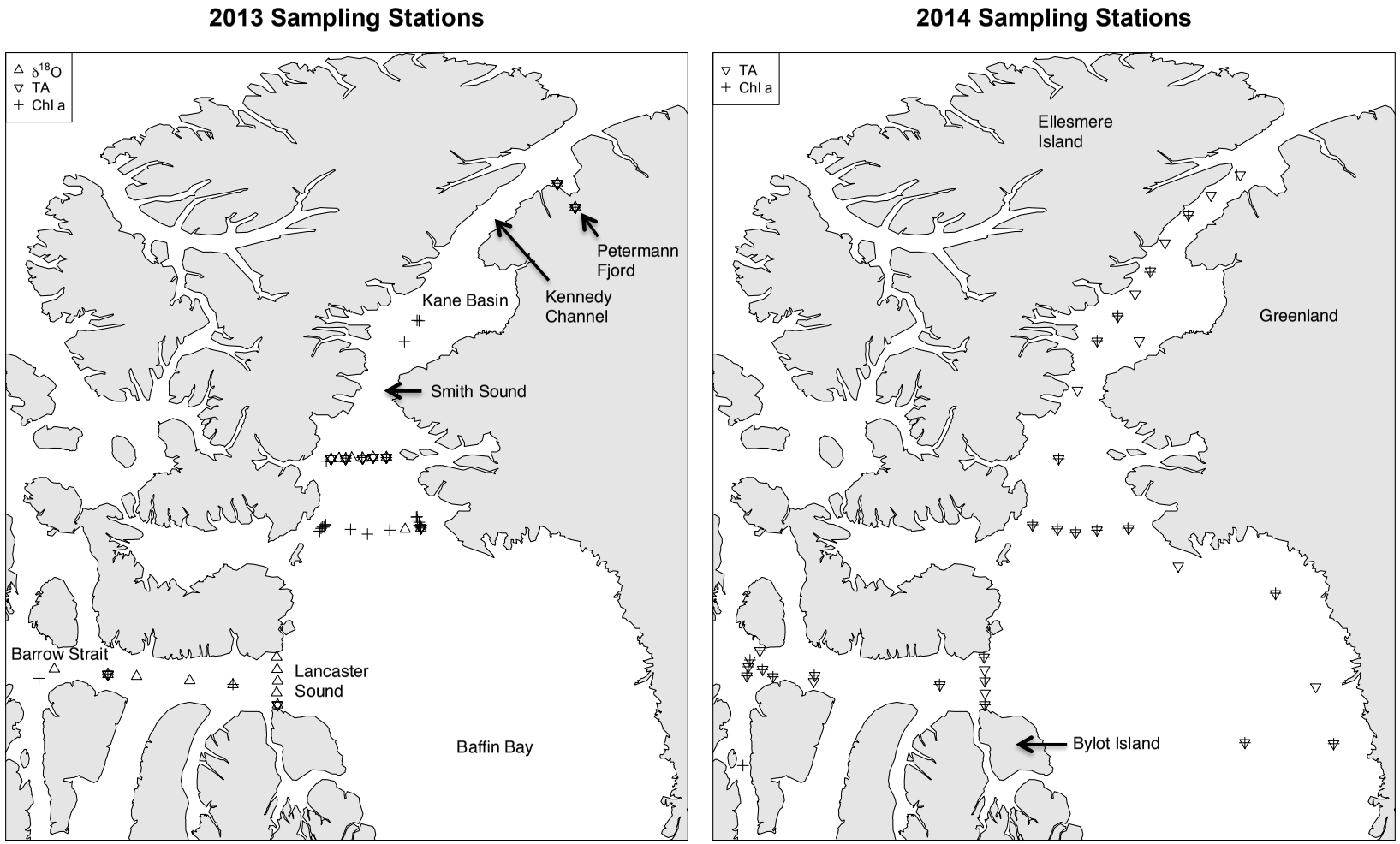

Figure 10: Sampling locations for ancillary measurements of $\delta^{18}O$ (upright triangle), TA/DIC (inverted triangle), and Chlorophyll-*a* (cross).

3.5.1 Carbonate System

The analysis of DIC and TA samples were conducted by two separate laboratories; 2013 samples were analyzed at Dalhousie University in Halifax, and 2014 samples at DFO's Institute for Ocean Sciences (IOS) in Sydney, British Columbia. Locations of sampling stations for both years are shown in Figure 10. Analysis of DIC and TA at Dalhousie was conducted by coulometric and potentiometric titration, respectively, using a VINDTA 3C (Versatile INstrument for the Determination of Titration Alkalinity) by Marianda and following standard procedures outlined in Dickson et al. [2007]. Analysis of DIC at IOS was conducted using a VINDTA 3D (essentially the DIC part of a VINDTA 3C) by coulometric titration and followed standard procedures [*Dickson et al.*, 2007]. TA analysis at IOS was conducted using a home-built system for open cell potentiometric titration, consisting of an automated Dosimat 665 titrator (Metrohm) and a Red Rod pH combination electrode (Radiometer Analytical). Endpoint detection was determined by a non-linear least squares fit following Dickson et al. [2007]. Both DIC and TA measurements were calibrated against certified reference materials (CRM 88, 115, 135) provided by Andrew Dickson (Scripps Institute of Oceanography). Analysis of DIC and TA samples at Dalhousie showed reproducibility better than +/- 1 and 2 μmol kg^{-1} respectively, whereas at IOS the uncertainties were +/- 1.3 and 3.6 μmol kg^{-1}, respectively.

3.5.2 Oxygen Isotopes

Samples for the determination of $\delta^{18}O$ were collected during the 2013 ArcticNet cruise and were analyzed at the GEOTOP-UQAM stable isotope laboratory at McGill University in Montreal. Oxygen isotopes were analyzed using the CO_2 equilibration method, where 200 μL of sample water was equilibrated with CO_2 for 7 h at 40 °C. The CO_2 was then collected and analyzed on a

Micromass Isoprime™ universal triple collector mass spectrometer in dual inlet mode with an AquaPrep™ system (Isoprime Ltd., Cheadle, UK). Results are expressed in the δ notation in ‰ versus Vienna Standard Mean Ocean Water (VSMOW). For each analytical sequence, two internal reference water samples were used to normalize the sample data ($\delta^{18}O = -6.71‰$ and −20.31‰). Uncertainties in replicate measurements are ± 0.05‰ (1σ).

3.5.3 Chlorophyll-a

Samples for the determination of chlorophyll-*a* were filtered through glass fiber filters (Whatmann GF/F) to capture the total (> 0.7μm) phytoplankton biomass. The filters were then inserted into a scintillation vial containing 10 mL of 90% acetone and are stored in the dark at 5 °C for 24 hours [*Hamilton*, 1984]. Fluorescence of the extract was then measured both before and after acidification with 100 mL of 5% HCl on a Turner Fluorometer (model 112).

3.6 Freshwater Decomposition

The varying chemical characteristics of different freshwater sources can be used to estimate fractional contributions from each source. Stable oxygen isotope ratios ($\delta^{18}O$) of seawater samples have been successfully used for decades to separate contributions of meteoric water from sea ice meltwater in various regions of the Arctic Ocean [*Tan and Strain*, 1980; *Östlund and Hut*, 1984; *Macdonald et al.*, 1995; *Schlosser and Newton*, 2002; *Alkire et al.*, 2015]. Assuming that each seawater sample is a mixture of seawater (SW), meteoric water (MW), and sea ice meltwater (SIM), conservation equations for salinity, $\delta^{18}O$, and mass (or volume) can be used provided end-member characteristics for each water type are known;

$$f_{SIM}S_{SIM} + f_{MW}S_{MW} + f_{SW}S_{SW} = S_{obs} \quad (14)$$

$$f_{SIM}\delta_{SIM} + f_{MW}\delta_{MW} + f_{SW}\delta_{SW} = \delta_{obs} \quad (15)$$

$$f_{SIM} + f_{MW} + f_{SW} = 1 \quad (16)$$

where f, S, and δ represent the fraction, salinity, and $\delta^{18}O$ respectively. Note that sea ice formation will generate a negative SIM fraction ($f_{SIM} < 0$).

The total alkalinity (TA) of different freshwater sources also varies significantly, making it another viable tracer of freshwater within the Arctic Ocean. River runoff (RR) contains relatively high TA in comparison to SIM and precipitation (see Figure 6). Yamamoto-Kawai et al. [2005] have demonstrated that TA is as effective a tracer as $\delta^{18}O$ for freshwater within the Arctic Ocean, and can be used in replacement of $\delta^{18}O$ (replace δ with TA) in the conservation equations (14) to (16). However, it is important to note that RR is used in replacement of MW when working with TA as a freshwater tracer.

In this study we utilize $\delta^{18}O$ measurements from the 2013 ArcticNet cruise, and TA measurements from the 2014 cruise to estimate freshwater fractions present in each year. Unfortunately due to data limitations we were unable to use the same tracer for both years. In past studies a three end-member system is assumed throughout the Arctic Ocean, with Atlantic water (ATL) typically representing the seawater component. The various freshwater sources contributing to the Arctic Ocean include SIM, RR, precipitation, and the salinity deficit of Pacific water. Using this framework, Pacific waters are represented as a mixture of ATL with MW or RR (depending on the tracer being used). This is because the salinity- $\delta^{18}O$ and salinity-TA properties of Pacific water lie on the mixing lines of ATL with MW or RR respectively

[*Ekwurzel et al.*, 2001]. Yamamoto-Kawai et al. [2005] found Pacific source waters to be characterized by MW or RR fractions of 7 – 11%.

In this investigation we originally began calculating freshwater fractions using the Atlantic seawater end-member, and found strong brine signals to be present throughout the study area. This is in agreement with past studies conducted in this area [*Yamamoto-Kawai et al.*, 2005; *Alkire et al.*, 2010; *Azetsu-Scott et al.*, 2012]. This strong brine signal is believed to originate in the central basins of the Arctic Ocean, and is advected into Baffin Bay through the channels of the CAA and Nares Strait. In order to determine if there were any local sea ice melt inputs, we must effectively subtract the predominant brine signal from these waters. To do this, we have chosen to use the salinity and $\delta^{18}O$/TA signal at the base of the surface mixed layer as our seawater end-member in equations (14) to (16). During summer it is assumed that any remaining winter water is located at the base of the surface mixed layer, indicated by the temperature minimum (T_{min}) throughout the depth profile. This winter water (WW) would represent the maximum brine signal produced over the past year. However, there are a number of different water masses interacting throughout our study area, and therefore the WW characteristics will vary between stations. We have identified four different water masses to be present, and therefore we have four different WW end-members that will be used to calculate freshwater fractions. We have adopted the naming convention of water masses presented in Bâcle et al. [2002], with Northern assembly (NA) waters derived from inflows through Nares Strait and Jones Sound; Southern assembly (SA) waters originating from the northward flowing WGC; North Water assembly (NWA) waters being a mixture of NA and SA waters in the vicinity of the NOW polynya; and we have added Western assembly (WA) waters entering northern Baffin Bay

via Barrow Strait and Lancaster Sound. End-member values for our freshwater decompositions are presented in Tables 1 and 2 for the years 2013 and 2014 respectively. All WW end-members were determined by averaging values of salinity and $\delta^{18}O$/TA found at the temperature minimum of the depth profile.

Table 1: Endmember definitions for 2013 freshwater decomposition.

Watermass	Salinity	$\delta^{18}O$ (‰)	Uncertainty (%)*
SIM	4 ± 1[a]	0.5 ± 2[a]	0.89
MW	0	-20 ± 2[b]	0.93
SA	33.5 ± 0.04	-1.23 ± 0.02	0.13
NWA	33.1 ± 0.1	-1.56 ± 0.02	0.34
WA + NA	32.5 ± 0.07	-2.06 ± 0.03	0.24

[a] Östlund & Hut, 1984
[b] Fairbanks, 1982
*Maximum uncertainty in water type fractions derived from varying salinity and $\delta^{18}O$ end-members within the limits of variability specified.

Table 2: End-member definitions for 2014 freshwater decomposition.

Watermass	Salinity	TA (µmol/kg)	Uncertainty (%)*
SIM	4 ± 1	263 ± 65[a]	0.40
MW	0	1412 ± 22[a]	0.23
NA	32.7 ± 0.20	2232 ± 4.5	0.97
SA	33.5 ± 0.06	2249 ± 21	1.68
NWA	33.1 ± 0.06	2247 ± 20	1.59
WA	32.0 ± 0.40	2202 ± 7	1.96

[a] Anderson et al. (2004)
*Maximum uncertainty in water type fractions derived from varying salinity and $\delta^{18}O$ end-members within the limits of variability specified.

3.7 Temperature Normalization

In order to investigate the sole effect of seawater temperature on pCO_{2sw} variations, pCO_{2sw} measurements were normalized to the mean T_{sw} observed throughout the study area (2 °C in both years) using the equation of Takahashi et al. [1993], such that;

$$npCO_{2sw} = pCO_{2sw} \cdot e^{0.0423(T_{mean} - T_{sw})} \quad (17)$$

where T_{sw} and pCO_{2sw} are our in-situ measurements, T_{mean} is equal to 2 °C, and $npCO_{2sw}$ are our normalized pCO_2 values. This calculation effectively removes localized effects of warming and cooling from our measurements of pCO_{2sw}, with the difference between pCO_{2sw} and $npCO_{2sw}$ representing the influence of temperature at any one point relative to the spatial mean.

4.0 RESULTS

4.1 PARAMETERS AT THE SEA SURFACE

Large spatial variability of surface water pCO_2 was observed throughout the study area in both years (Figure 11). During 2013 the lowest observed value of pCO_{2sw} (144.8 µatm) was located just off the east coast of Devon Island, with another pocket of very low pCO_{2sw} near the

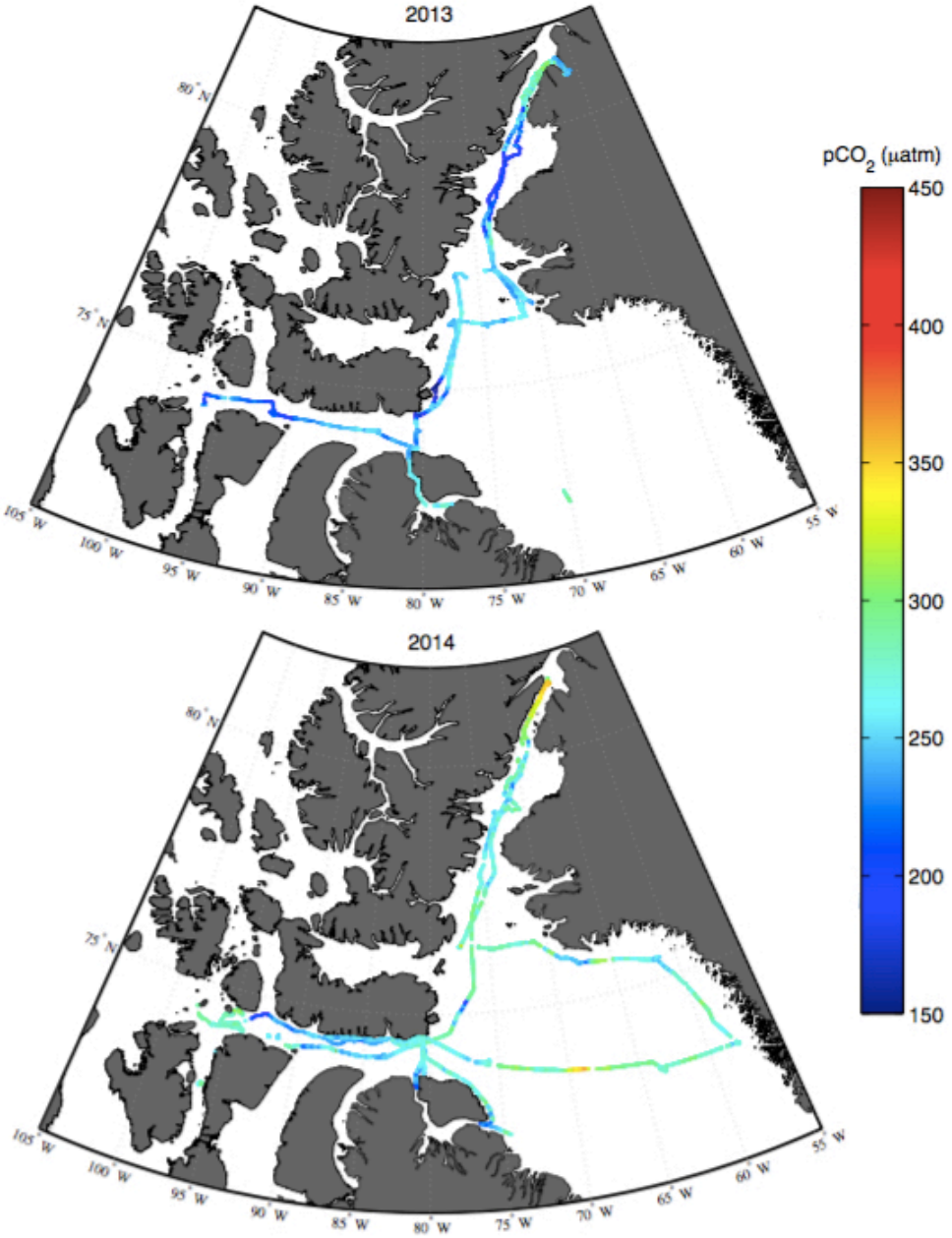

Figure 11: Continuous underway pCO_{2sw} measurements collected in summer 2013 and 2014.

south-eastern tip of the island. Other areas of low pCO_{2sw} (< 250 µatm) include Kane Basin, Barrow Strait, and Petermann Fjord (see Figure 10 for location names). The highest observed pCO_{2sw} in 2013 (312.3 µatm) was found in Kennedy Channel, and gradually decreased southwards in Nares Strait.

In 2014 the lowest recorded measurement of pCO_{2sw} (165.2 µatm) was located between Bylot Island and Baffin Island near the community of Pond Inlet. Similar to 2013 other areas presenting very low pCO_{2sw} were located in Barrow Strait, Kane Basin, and east of Devon Island. The 2014 cruise traversed northern Baffin Bay revealing pockets of low pCO_{2sw} along the west coast of Greenland. High pCO_{2sw} was again observed in Kennedy Channel (361.9 µatm) as well as in the center of northern Baffin Bay (364.0 µatm). All recorded pCO_{2sw} measurements during both years were lower than atmospheric levels, indicating that this entire oceanographic region is undersaturated in pCO_2.

Large variability was also present in measurements of surface seawater temperature (T_{sw}) and salinity (Figures 12 and 13). Generally, areas exhibiting low pCO_{2sw} are found to coincide with regions of low T_{sw} (< 0°C) and low salinity (< 30). Oftentimes significant sea ice cover is also present in these areas signaling the influence of SIM or under-ice productivity. However, there are some exceptions, such as along the west coast of Greenland where warm T_{sw} and high salinity occur with low pCO_{2sw}. In past studies high pCO_{2sw} has commonly been found in areas of upwelling, displaying both increased salinity and T_{sw} [*Bâcle et al.*, 2002; *Fransson et al.*, 2009; *Else et al.*, 2013a; *Evans et al.*, 2015]. This seems to be the case in 2014 near the center of northern Baffin Bay, where we observed an area of relatively high pCO_{2sw}. However, in the case

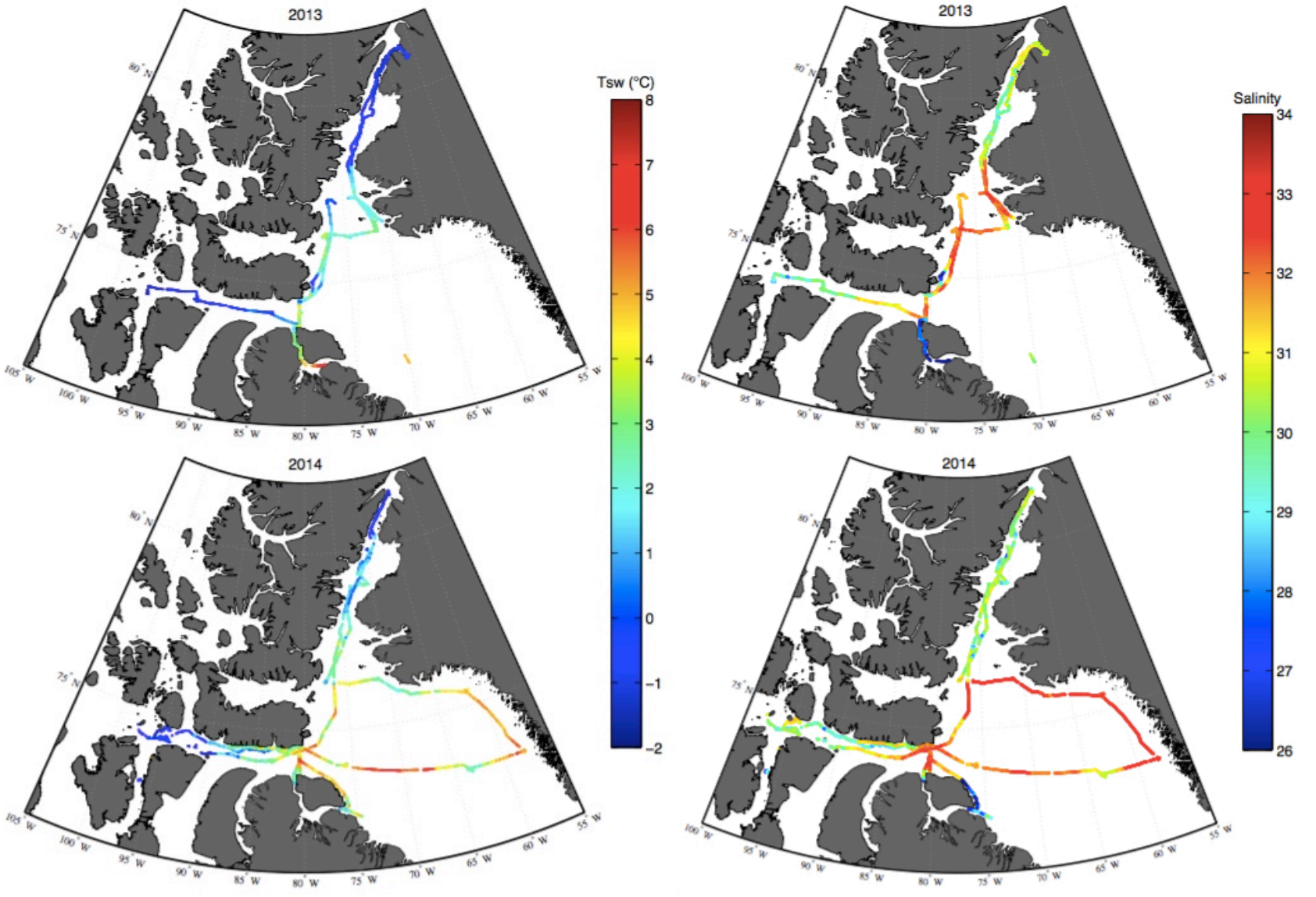

Figure 12: Underway measurements of surface seawater temperature (T_{sw}) and salinity collected during summer of 2013 and 2014.

of Kennedy Channel (which also displayed relatively high pCO_{2sw}) neither T_{sw} nor salinity are high, indicating that upwelling is not the cause of increased pCO_{2sw} in this area.

Figure 13 presents our underway pCO_{2sw} measurements in temperature-salinity space, allowing for greater distinction between water masses and various freshwater sources, and their resultant impacts on pCO_{2sw}. Within Figure 13 the study area has been partitioned into four sub-areas, (1) Baffin Bay, defined here as east of 80 °W and south of 76 °N, (2) Lancaster Sound and Barrow Strait, defined by measurements west of 80 °W (also includes measurements between Bylot and Baffin Islands), (3) the North Water (NOW) region, defined by measurements between 76 °N and 78 °N, and finally (4) Nares Strait, containing all measurements north of 78 °N. Figure 13 reveals many areas of especially low pCO_{2sw} coinciding with cold T_{sw} and low salinity, but also some areas of higher pCO_{2sw}. Higher pCO_{2sw} was observed in central northern Baffin Bay (Figure 13b) coinciding with high T_{sw} and salinity, signaling an area of upwelling. The highest pCO_{2sw} measurements were recorded in 2013 within Kennedy Channel (Figure 13h), however neither salinity nor T_{sw} is especially high in this area. Another area of somewhat increased pCO_{2sw} was observed between Bylot Island and Baffin Island in 2013 (Figure 13c), here T_{sw} is high and salinity is low and we hypothesize that this may be due to riverine input from the nearby Mary River on Baffin Island.

Sea ice coverage was found to be extremely variable in both years. During 2013 high concentrations of ice floes (6 to 7 tenths) were observed within Kane Basin and Kennedy Channel. In these northern reaches of Nares Strait the sea ice consisted of a mixture of first-year and multi-year ice floes, along with occasional icebergs originating from the glaciers of

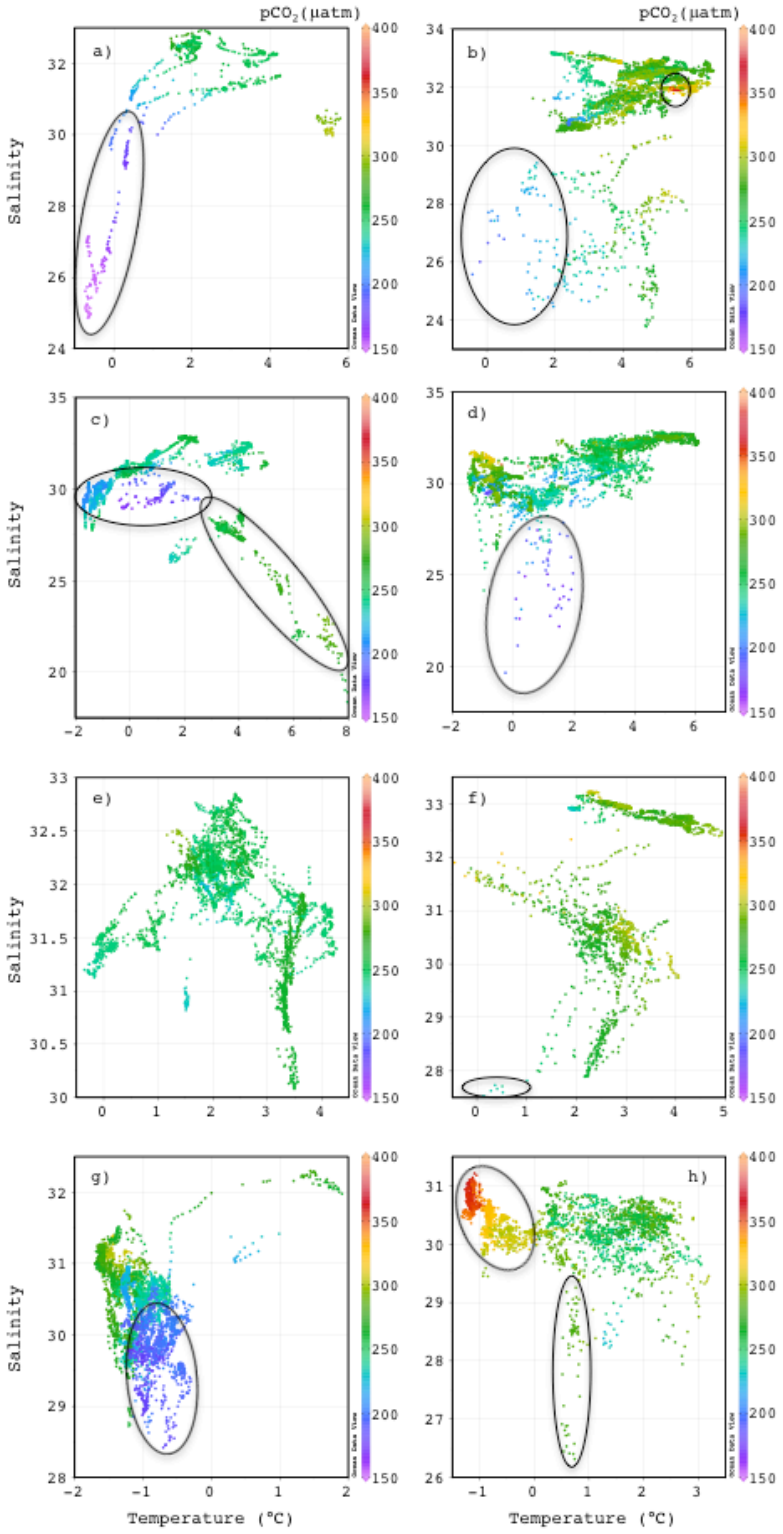

Figure 13: pCO_{2sw} measurements from 2013 (left column) and 2014 (right column) presented in temperature-salinity space in Baffin Bay (a,b), Lancaster Sound and Barrow Strait (c,d), the NOW polynya region (e,f), and Nares Strait (g,h). Circled areas represent regions of freshwater inputs and/or upwelling contributing to significant fluctuations in pCO_{2sw}. Axes have been scaled to show trends.

Greenland or Ellesmere Island. In contrast, during July 2014 the ice arch of the NOW polynya was still present within Kennedy Channel, leaving Kane Basin and the NOW polynya region to the south largely ice-free. The ice arch began its break-up during late July, and by the time of sampling in this area (Aug 3-6, 2014) had retreated to the northern reaches of Kennedy Channel. The remainder of our study area was mainly ice free in both years, with the exception of Barrow Strait where low concentrations (1 to 5 tenths) of first-year ice were observed in 2013, and in 2014 higher coverage (5 to 9 tenths) extended east to approximately 89 °W.

4.2 Rates of Air-Sea CO_2 Exchange

Variable wind speeds were observed throughout the eastern Canadian Arctic, with remarkably similar distributions recorded in each year. During 2013 the average wind speed (adjusted to a height of 10 m) was 4.07 m s^{-1} with a minimum and maximum recorded wind speed of 0.34 m s^{-1} and 12.25 m s^{-1} respectively; and in 2014 the average wind speed was 4.66 m s^{-1}, with a minimum and maximum of 0.23 m s^{-1} and 14.38 m s^{-1} respectively.

Figure 14 shows calculated air-sea CO_2 fluxes (mmol C m^{-2} d^{-1}) adjusted for sea ice concentration, with negative values denoting a sink of CO_2 (absorption by the surface ocean) and positive values indicating a source of CO_2 (outgassing to the atmosphere). Due to the consistent undersaturation of surface waters ($pCO_{2sw} < pCO_{2atm}$), the entire region was found to be a sink of atmospheric CO_2 during both years. The greatest rates of CO_2 uptake were -44.6 mmol m^{-2} d^{-1} in 2013 found off the east coast of Devon Island, and -45.5 mmol m^{-2} d^{-1} in 2014 located in Barrow Strait. Average calculated CO_2 fluxes for 2013 and 2014 were -6.6 and

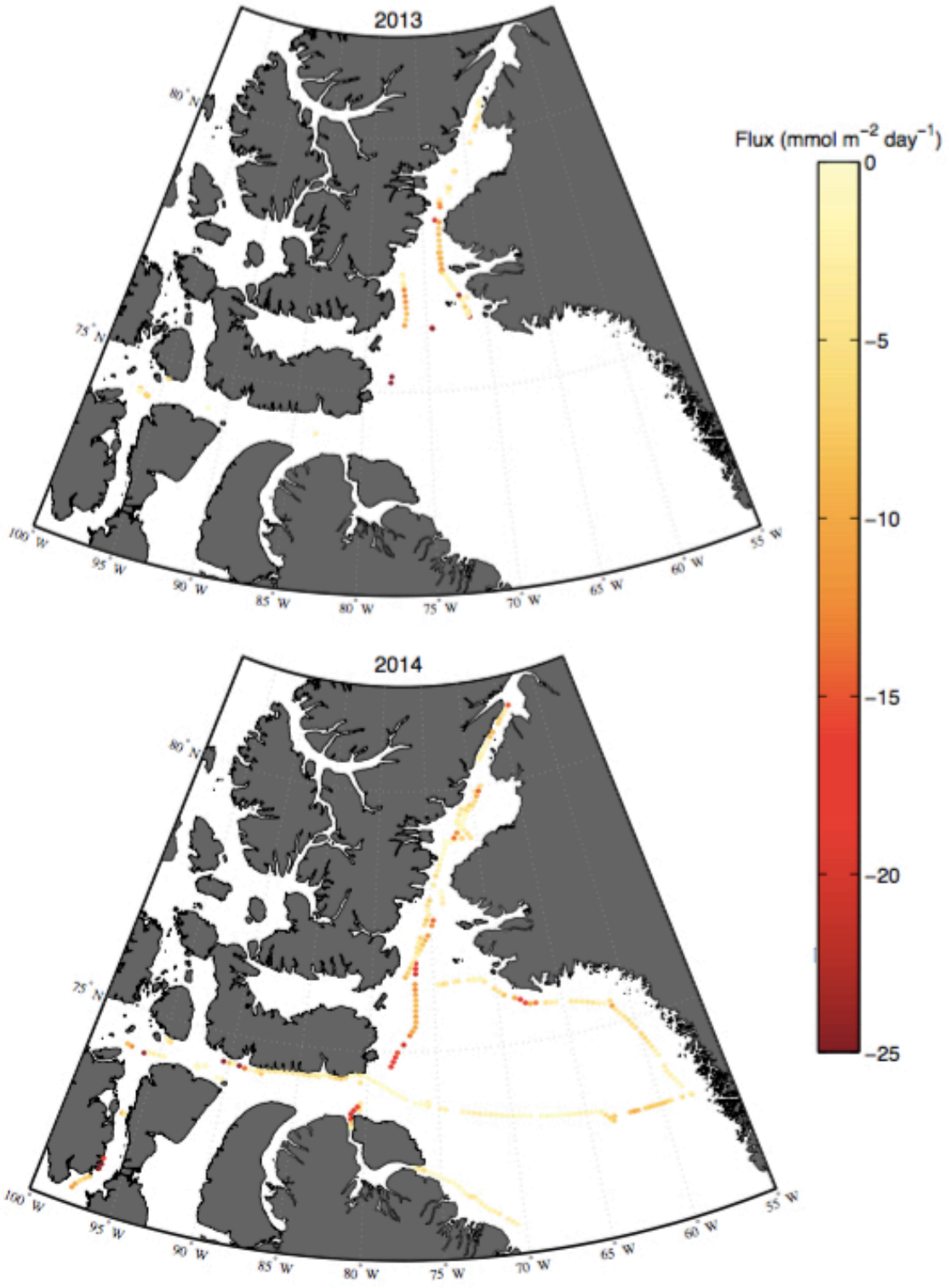

Figure 14: Calculated rates of air-sea CO_2 exchange within the eastern Canadian Arctic. Negative values denote oceanic uptake of atmospheric CO_2.

-5.2 mmol m^{-2} d^{-1}, respectively. Stronger rates of air-sea CO_2 exchange were not always observed in areas where the ocean-atmosphere pCO_2 gradient was greatest. Wind speed plays a large role in determining instantaneous rates of air-sea exchange, as it determines the magnitude of the transfer velocity. In this investigation strong air-sea CO_2 fluxes within the NOW Polynya region and Kennedy Channel during 2014 were largely the result of persistent high wind speeds recorded in these areas. Unfortunately, during the 2013 cruise winds were often blowing from the stern of the vessel and were therefore screened out of the data utilized in CO_2 flux calculations. Winds originating from the stern of the ship become distorted by the ship body, leading to inaccurate measurements of wind speed by sensors located at the bow of the ship.

4.3 Processes controlling the distribution of pCO_{2SW}

4.3.1 Water Masses

The characteristics of different water masses play a large role in determining surface water pCO_2, and depend upon the sources and histories of those water masses. In very general terms, all water masses within the eastern Canadian Arctic can be described as a mixture of either Arctic waters ($T < 0°C$; $S < 34$) entering from the north via Nares Strait or from the west through the CAA, and Atlantic waters ($T > 0°C$; $S > 34$) entering Baffin Bay from the south via the WGC [*Bâcle et al.*, 2002; *Melling et al.*, 2010]. Arctic waters may be a mixture of Pacific (PW) and Atlantic (ATL) source waters that have circulated the Arctic Ocean prior to exiting to the North Atlantic. By first preforming our freshwater decomposition using ATL ($S = 34.87$, $\delta^{18}O = 0.24$, $TA = 2306$) as our SW end-member (following end-member values used by Yamamoto-Kawai et al. [2005]), we were able to locate PW throughout the region, as PW contains roughly 7 to 11% more MW/RR compared to Atlantic water [*Yamamoto-Kawai et al.*,

2005]. MW and RR fractions above 11% were assumed to be additional contributions from Arctic rivers, and were investigated further using WW end-members, this will be discussed later in section 4.3.3.

The distribution of PW was found to be similar in both years, occupying the upper water column within Barrow Strait, Lancaster Sound, and the western side of the NOW Polynya (location of the BIC); and the absence of PW along the western coast of Greenland (location of the WGC) and the eastern half of the NOW polynya region. During 2013 PW was found to depths of 200 m in western Barrow Strait and gradually shallowed to 150 m approaching Lancaster Sound. However, in 2014 the depth of PW in Barrow Strait was increasingly shallow (100 m), being confined to the surface mixed layer (50 m depth) in the center of Lancaster Sound. In both years intrusions of Atlantic water were found at depth in the center of Lancaster Sound, with PW largely confined to the northern and southern edges of the transect. This intrusion was found to be significantly larger in 2014 and appears to extend further into Barrow Strait compared to 2013. Evidence of this intrusion can also be seen in surface salinity and T_{sw} measurements (see Figure 14), which both increase due to the presence of ATL. During 2014 PW was also found to occupy the upper water column of Nares Strait, extending to depths of 100 m within Kennedy Channel (northern end of Nares Strait), but becoming confined to the surface mixed layer (50 - 60 m) after passing over the shallow sill within Kane Basin. These results suggest that Arctic waters flowing into Baffin Bay via Nares Strait and the CAA are derived of both ATL and PW, with PW occupying the upper water column (depths <= 150 m).

While the temperature and salinity characteristics of Arctic outflow and ATL vary greatly, their TA and DIC concentrations differ only marginally (also found by Miller et al. [2002]), with ATL having only slightly higher TA and DIC compared to Arctic waters. Therefore, significant differences in pCO_{2sw} between these water masses are likely derived from other factors, such as the influence of temperature, biology, or freshwater inputs within the surface mixed layer.

4.3.2 Temperature Variations

Figure 15 shows temperature-normalized values of pCO_{2sw} ($npCO_{2sw}$), which effectively remove the influence of temperature variations on measurements of pCO_{2sw}. Therefore, variations in $npCO_{2sw}$ highlight areas where other factors (e.g biology, freshwater inputs) are significantly contributing to pCO_{2sw} variations. We can see from Figure 15 that the high pCO_{2sw} previously observed in the center of northern Baffin Bay is no longer present, signaling that these high pCO_{2sw} measurements were largely due to temperature variations (specifically an increase in temperature). However, pockets of low pCO_{2sw} remain within Kane Basin and along the coast of Devon Island in 2013, as well as along the west coast of Greenland and in Barrow Strait during 2014. This suggests that these areas of low pCO_{2sw} are not solely the result of decreasing temperatures, and are likely due to significant fluctuations in TA and DIC associated with SIM or glacial meltwaters. Figure 15 also illustrates the persistence of high pCO_{2sw} within Kennedy Channel during both years, suggesting that temperature is not playing a significant role in this area, and the relatively high pCO_{2sw} in this location is due to other factors.

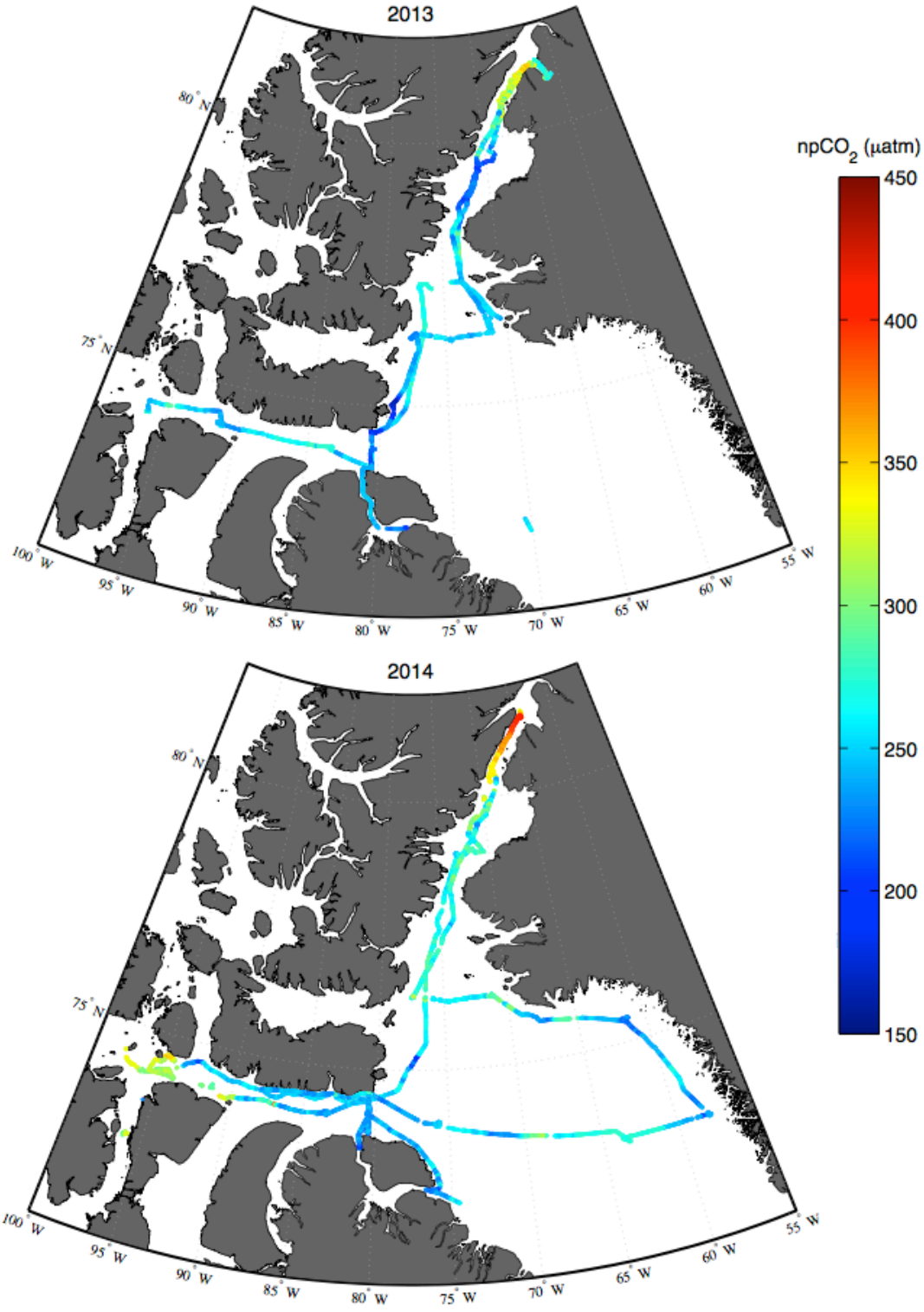

Figure 15: Variations in $npCO_{2sw}$ (temperature-normalized pCO_{2sw}) throughout the eastern Canadian Arctic during summer of 2013 and 2014.

4.3.3 Freshwater Inputs

By utilizing WW characteristics of each water mass as seawater end-members in equations (14) to (16) we were able to estimate local contributions of SIM and MW/RR present within the surface mixed layer. Figure 16 shows calculated surface freshwater fractions during 2013 and 2014. Only two areas were found to exhibit significant SIM; Barrow Strait and along the western coast of Greenland. Observations of sea ice coverage confirm the presence of sea ice within Barrow Strait during both years, however no sea ice was observed within Baffin Bay. Upon further inspection, SIM within eastern Baffin Bay was found to occupy the entire surface mixed layer, with low positive fractions extending to depths of 100 m near the halocline (see Figure 17). This provides evidence that this strong SIM signal is being advected into eastern Baffin Bay, carried by the WGC. The large quantities of SIM observed are likely remnants of the EGC, which transports large quantities of sea ice south from Fram Strait along the east coast of Greenland. The EGC flows geostrophically around the southern tip of Greenland, feeding into the WGC at its point of origin. The large positive fractions of SIM carried by the WGC gradually decline within the NOW polynya region, where the WGC mixes with Arctic waters of the BIC. Smaller positive fractions of SIM are observed within the NOW polynya and in Kane Basin during 2014, and are perhaps caused by the episodic break-up of the ice arch within Kennedy Channel. Kennedy Channel itself is found to contain no SIM, indicating that the ice arch was not melting significantly while present in this area. Unfortunately no sampling for $\delta^{18}O$ was conducted within Kane Basin or Kennedy Channel in 2013, so we are unable to calculate freshwater fractions in these areas. However, based on sea ice observations (and in-situ T_{sw} and salinity measurements) it is highly likely that large positive fractions of SIM would be present

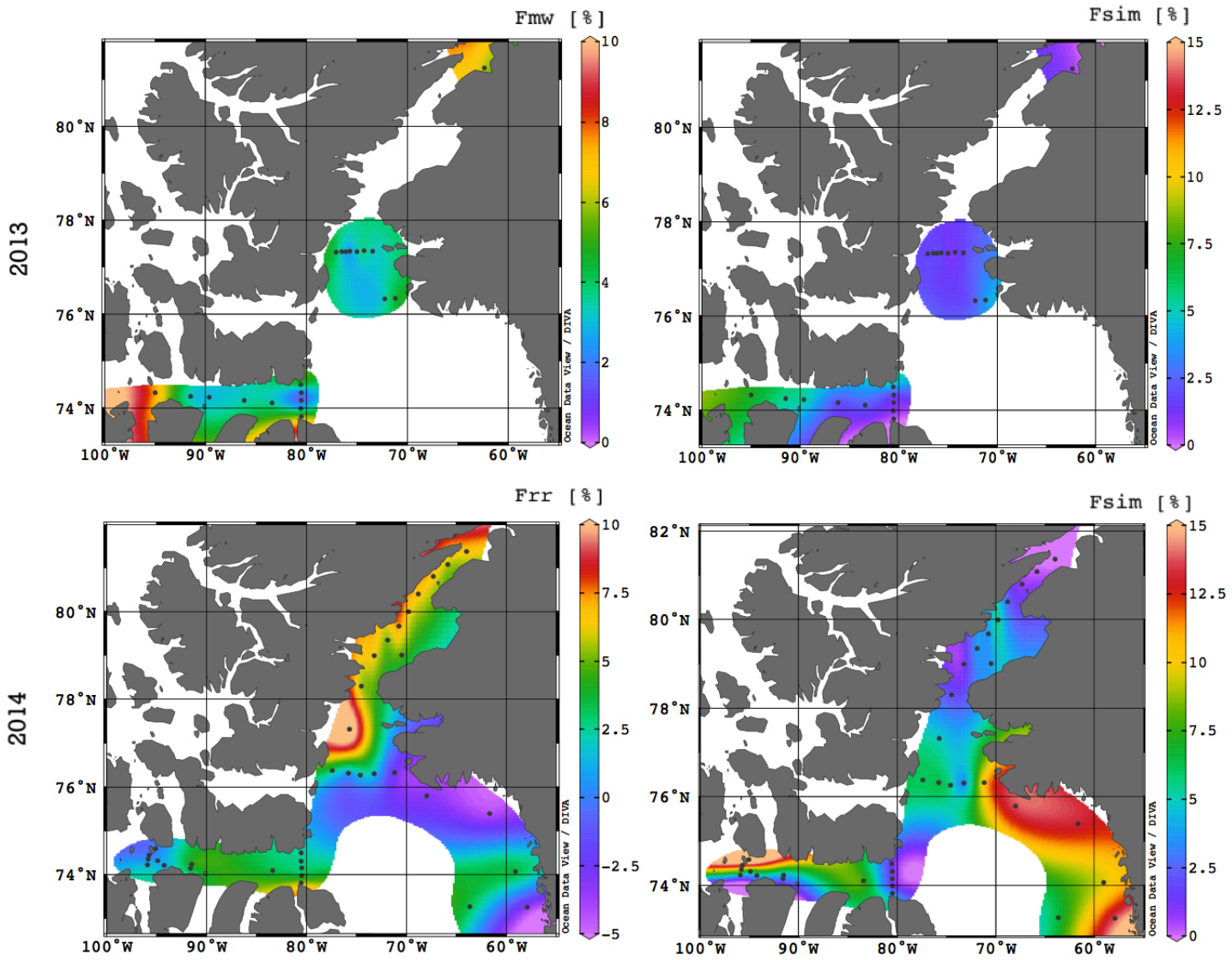

Figure 16: Calculated surface freshwater fractions based on $\delta^{18}O$ (2013) and TA (2014) samples collected at discrete sampling stations (indicated by black dots).

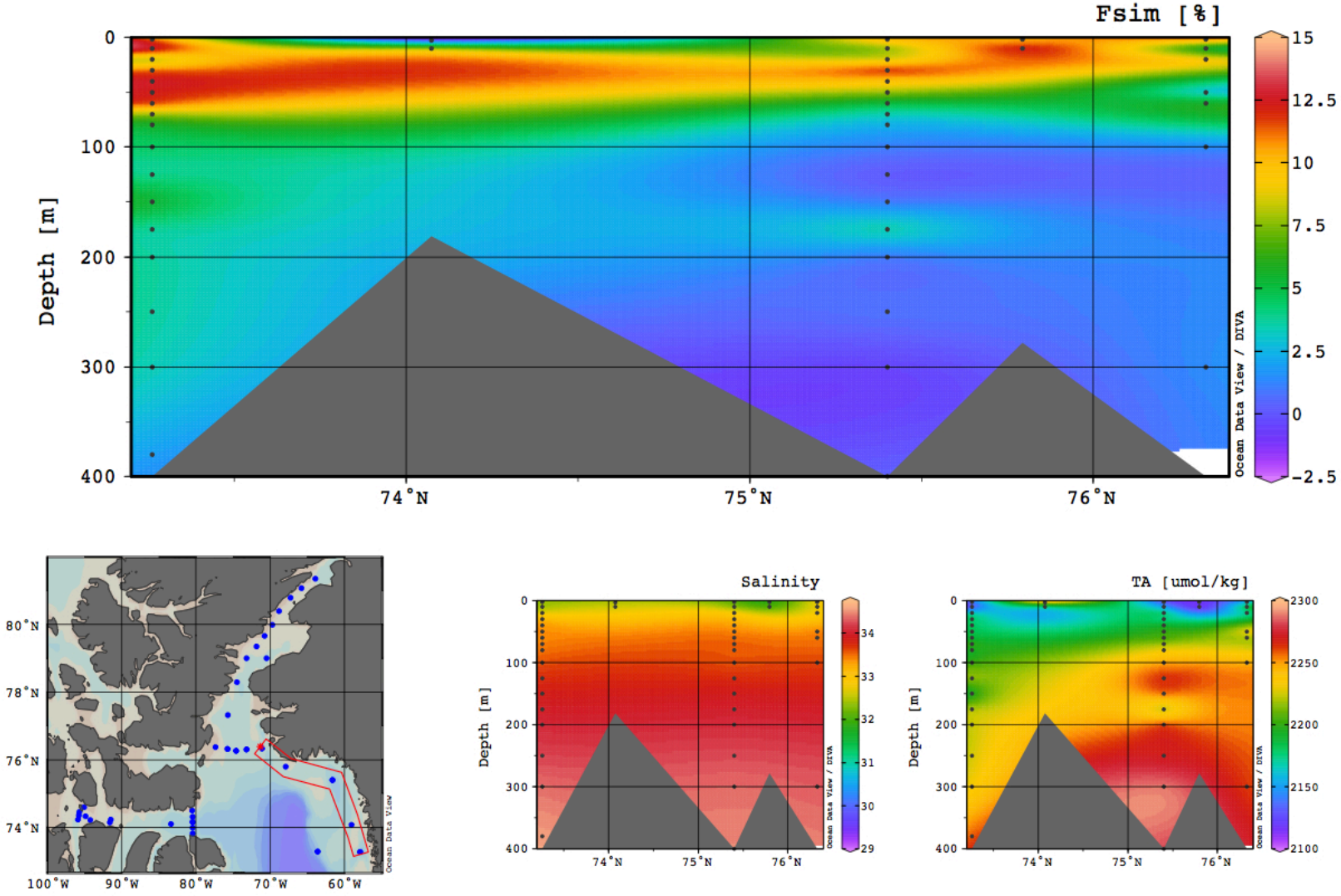

Figure 17: Fractions of sea ice melt (F_{sim}) throughout the surface mixed layer of eastern Baffin Bay. The inset map shows the locations of sampling stations in this area. Inset plots show salinity and TA measurements used in the calculation of freshwater fractions.

within both Kane Basin and Kennedy Channel in 2013. Our only sampling stations near these areas in 2013 were conducted within Petermann Fjord, which is a 1100m deep fjord separated from the waters of Nares Strait by a 350 - 450 m deep sill [*Johnson et al.*, 2011] and is the termination point of the Petermann Glacier. We found the surface waters within Petermann Fjord to contain no SIM, but did contain significant MW fractions due to glacial ice melt.

Calculated fractions of MW in 2013 and RR in 2014 show some similarities, with positive fractions located both in Barrow Strait and at the southern edge of the Lancaster Sound transect. River water may be transported from as far as the Mackenzie or Yukon rivers through the channels of the CAA to end up in Barrow Strait and/or Lancaster Sound. There are also many other small Arctic rivers located on the islands of the CAA that may contribute riverine inputs to this area. Near the community of Pond Inlet (between Bylot and Baffin Islands) is the mouth of the Mary River, which may contribute to the increased MW observed at the southern edge of Lancaster Sound. Based on the interpolated results displayed in Figure 16, it appears that there are similar positive fractions located in northern Nares Strait during both years. However, the only sampling stations in this area during 2013 were located in Petermann Fjord, and are more likely to be influenced by glacial ice melt than the 2014 stations in the center of Nares Strait. The greater number of sampling stations throughout Nares Strait in 2014 revealed positive fractions of RR throughout the area. The four northern-most sampling stations within Kennedy Channel displayed RR fractions between 5-7% throughout the surface mixed layer to depths of ~50 m (see Figure 18). Similar to SIM in eastern Baffin Bay, the presence of these significant RR fractions at depth indicates the advection of a water mass carrying this signal into Kennedy Channel. The salinity of this water mass ranges between 30.7 and 31.8, indicating that the water

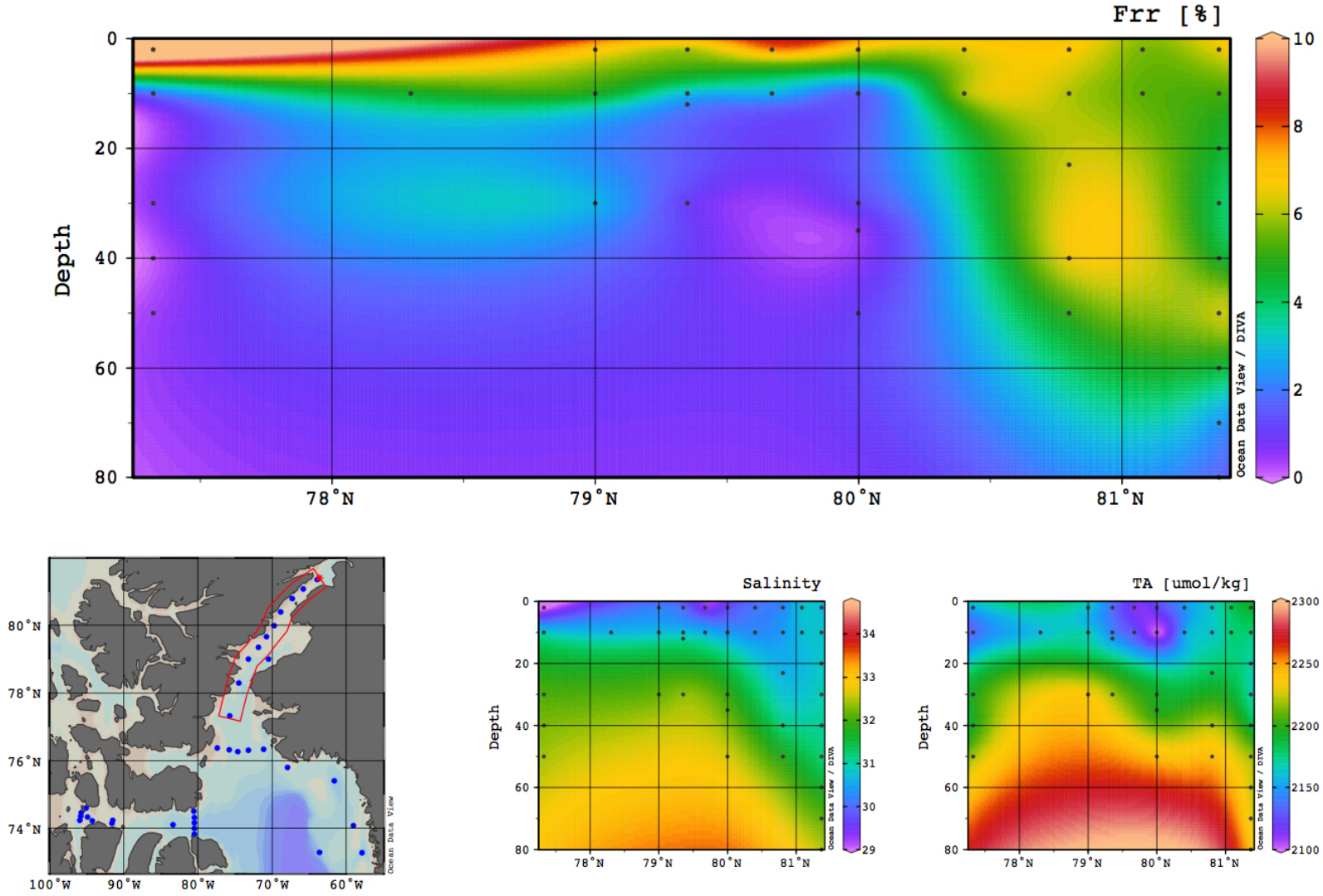

Figure 18: Fractions of river runoff (F_{rr}) within Nares Strait, the four most northerly stations in this transect represent Kennedy Channel. The inset map shows station locations in this area. Inset plots show salinity and TA measurements used in the calculation of freshwater fractions.

is of Pacific origin. Following the descriptions of Pacific water masses described by Steele et al. [2004] Alaskan coastal water (ACW) fits this salinity range (commonly defined by $31 < S < 32$), and is typically characterized by significant riverine influence (especially from the Yukon river). ACW is transported from its origin in the Bering Sea eastwards along the continental slope by the North American boundary current. Portions of ACW may spin off as eddies into the Canada Basin, however the remainder continues along the North American continental slope, and has been observed as far east as the Lincoln Sea north of Ellesmere Island [*Newton and Sotirin*, 1997]. The observed plume of ACW within Kennedy Channel abruptly ends near the entrance to Kane Basin, the location of a 250 m deep sill. It is uncertain whether the sill has any impact on the advection of the ACW, however south of this point high RR fractions are only found at the surface. The positive RR fractions throughout the remainder of Nares Strait may also be related to the ACW, or may be local contributions from smaller rivers and glacial inputs from Ellesmere Island and/or Greenland.

Interestingly, some negative RR fractions were calculated in 2014 within the surface layer of east Baffin Bay (note change in scale in Figure 16), coinciding with high positive fractions of SIM advected by the WGC. In the natural world negative fractions of RR have no physical representation, however within the framework of our three end-member freshwater decomposition model negative RR fractions are possible if our water sample exhibits a lower TA than that of SIM. This is similar to how negative fractions of SIM can occur when water samples fall below the MW-SW mixing line in salinity- $\delta^{18}O$ space. Here our negative RR fractions are occurring in TA-salinity space and therefore must fall below the SIM-SW mixing line. The only known freshwater input that may contain less TA than SIM is glacial ice melt. Meire et al.

[2015] measured the TA from several icebergs within Godthåbsfjord in west Greenland, and characterized glacial ice melt as having a TA of 50 ± 20 μmol kg^{-1}. Based on this, it is hypothesized that the negative RR fractions within eastern Baffin Bay may be indicative of glacial ice melt input at the surface. The $\delta^{18}O$ of glacial ice melt is more negative than that of MW, and therefore would result in both positive fractions of MW and negative fractions of SIM in salinity- $\delta^{18}O$ space. Johnson et al. [2011] estimated the $\delta^{18}O$ of glacial ice melt from the Petermann Glacier to be -27 ‰ using a linear regression of water samples from Petermann Fjord. When preforming our freshwater decomposition with ATL as our SW end-member, both negative fractions of SIM and high positive MW fractions are found at the surface of Petermann Fjord, indicating the presence of glacial ice melt. Negative fractions of SIM are not observed in Petermann Fjord when using WW end-members, as WW characterizes the maximum brine signal within the water column and effectively represents this as seawater.

4.3.4 Primary Productivity

Surface waters within the eastern Canadian Arctic are found to display low rates of primary productivity, with chlorophyll-*a* concentrations (Chl-*a*) ranging between 0.1 and 2.3 μg L^{-1}. Low surface Chl-*a* concentrations are common during the summer season, as the initial spring phytoplankton bloom depletes the surface mixed layer of its nutrients. Further, large freshwater inputs throughout the spring and summer seasons create strong stratification within the surface layer, preventing the replenishment of nutrients from deeper waters [*Carmack et al.*, 2004; *Tremblay et al.*, 2008]. Surface waters displaying slightly higher Chl-*a* concentrations (1.2 – 2.3 μg L^{-1}) were observed in Barrow Strait and Kane Basin in close proximity to melting first-year ice floes. In these locations it is likely that SIM provides a weak source of nutrients at the surface. One significant exception was found within Petermann Fjord, where higher Chl-*a*

concentrations were observed at the surface ranging between 8.0 µg L^{-1} near the termination point of the glacier to 5.1 µg L^{-1} near the entrance to Nares Strait. Here glacial ice melt may be delivering a constant source of nutrients to the surface mixed layer, allowing the phytoplankton bloom to persist throughout the summer season.

Due to the depletion of nutrients within the surface mixed layer, it is common in the Arctic Ocean to observe subsurface chlorophyll-*a* maxima (SCMs). These SCMs are generally found to coincide with the position of the nitracline (a strong gradient in dissolved inorganic nitrogen) where both sufficient light and nutrients are available for primary production [*Ardyna et al.*, 2013]. Several SCMs were detected from chlorophyll-a measurements during the 2013 cruise, the strongest of which (5.74 µg L^{-1}) was located between 20 – 40 m depth within the northeast NOW polynya region (Figure 19).

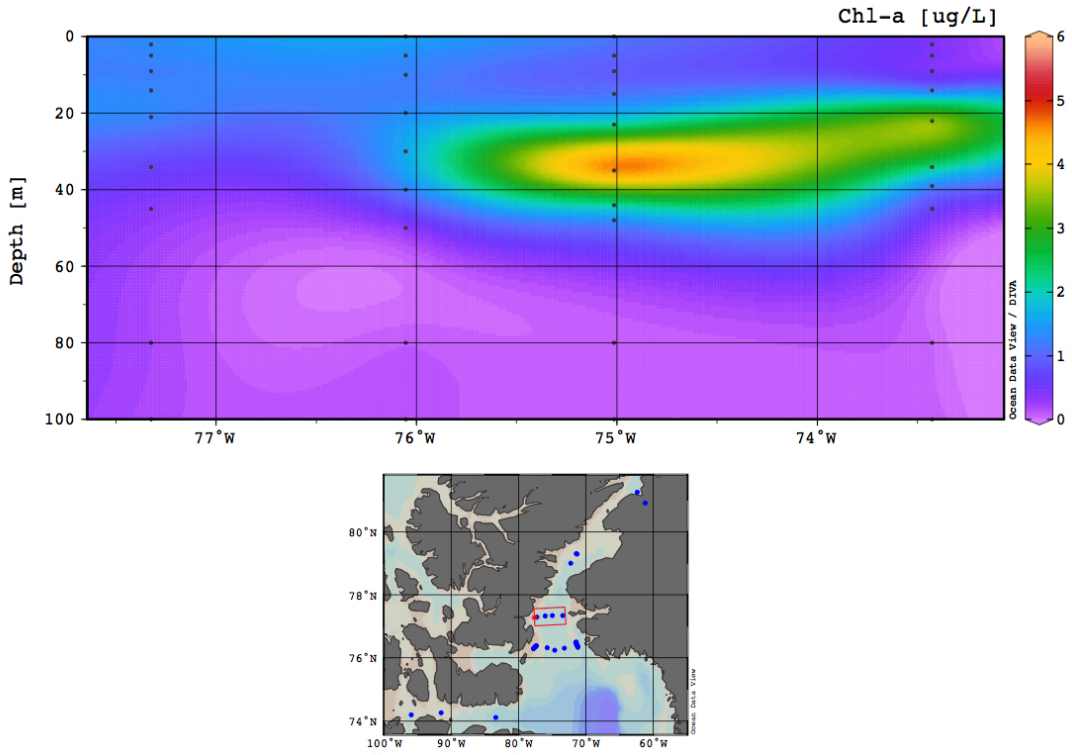

Figure 19: Subsurface chlorophyll-a maximum (SCM) located in the northeastern NOW polynya region in 2013. Inset map shows sampling station locations in this area.

5.0 DISCUSSION

Perhaps the most unexpected observation of this investigation was the location of the highest recorded pCO_{2sw} values within Kennedy Channel. Using TA and salinity measurements collected in 2014 these high pCO_{2sw} values were linked to the presence of Alaskan Coastal Water (ACW) in the upper water column, which carries a strong riverine signal originating from the Yukon River [*Steele et al.*, 2004]. Using fluorescence measurements this water mass was also found to exhibit large amounts of chromophoric dissolved organic matter (CDOM) ranging from 10.5 to 11.5 mg m^{-3}. High amounts of CDOM within the water column limits light availability for primary producers such as phytoplankton, as it strongly absorbs short-wavelength (blue) light in the same range where chlorophyll-a has an absorption peak [*Arrigo and Brown*, 1996]. Therefore, the high pCO_{2sw} measurements found within ACW may be indicative of a net-heterotrophic environment induced by large amounts of CDOM. CDOM will undergo photo-degradation in the presence of sunlight, and therefore the high concentrations found in Kennedy Channel will likely subside over time. Such high amounts of CDOM likely persisted in this water mass due to the presence of the NOW polynya ice arch in Kennedy Channel, which would limit the amount of sunlight entering the water column.

5.1 INFLUENCE OF THE ARCTIC OSCILLATION

ACW must be transported great distances from its origin in the Bering Sea in order to reach the waters of Nares Strait. The circulation patterns of ACW have been linked to surface wind fields and the Arctic Oscillation (AO), with strongly positive AO periods leading to the arrival of ACW north of Ellesmere Island [*Steele et al.*, 2004]. During periods of positive AO the anti-cyclonic surface circulation of the Beaufort Gyre is weakened, allowing for the greater eastward flow of

the ACW by the North American boundary current. On the other hand, during periods of negative AO the Beaufort Gyre is intensified, hindering the eastward flow of ACW along the continental margin. Using monthly mean AO indices from the NOAA Climate Prediction Center (http://www.cpc.ncep.noaa.gov) we found AO indices within early (JFM) 2014 to be positive, whereas in early 2013 AO indices were negative. The positive AO period in early 2014 may have contributed to the increased transport of ACW into Nares Strait, leading to the observed increase in pCO_{2sw} within Kennedy Channel.

Positive phases of the AO also cause an enhancement of the transpolar drift stream (TDS), a wind-driven circulation feature of the Arctic Ocean that transports surface waters from northern Siberia across the Arctic Ocean towards Greenland. An enhancement of the TDS in early 2014 may have directly contributed to the strong SIM signal found in eastern Baffin Bay by exporting large amounts of sea ice from the Arctic Ocean via Fram Strait. Most of the exported sea ice would melt while being carried southwards by the EGC, eventually feeding into the WGC to be transported into Baffin Bay. Surface pCO_{2sw} values in eastern Baffin Bay would likely be significantly higher in the absence of this strong SIM signal, especially due to the warmer temperatures and relatively high DIC of Atlantic waters.

5.2 The Role of Glacial Ice Melt

In 2013 the CCGS Amundsen ventured as far north as Petermann Fjord, where surface waters were found to contain lower pCO_{2sw} in comparison to the adjacent waters of Nares Strait. This was discovered to be related to the presence of a significant phytoplankton bloom within the surface waters of the fjord. A recent study by Bhatia et al. [2013] suggests that large amounts of

bioavailable iron are delivered to the surface ocean from several land-terminating glaciers within western Greenland. Iron is a micronutrient required for primary production that is normally in short supply throughout surface waters of the Arctic Ocean, and therefore a large enhancement of bioavailable iron would almost certainly increase rates of primary production within Arctic waters. Despite the fact that the Petermann Glacier is a tidewater glacier (terminating over water), it may still be capable of delivering large amounts of iron into the fjord through the strong discharge of basal meltwater carrying high sediment loads [*Johnson et al.*, 2011]. Depending on the depth of basal meltwater release this glacial meltwater may also induce mixing and transport of deep nutrient-rich waters to the surface. As the melt of the Greenland ice sheet continues to escalate with warmer surface air temperatures [*Rignot et al.*, 2011; *Bamber et al.*, 2012], it is likely that glaciers will represent an increasing source of bioavailable iron to surface coastal oceans throughout the Arctic.

Glacial ice melt may also play a role in the lowest recorded measurements of pCO_{2sw} along the east and southern coasts of Devon Island, as these pockets of low pCO_{2sw} coincide with locations of glacial tongues of the Devon ice cap. As previously mentioned, it is hypothesized that negative calculated RR fractions within eastern Baffin Bay are indicative of the extremely low TA of glacial meltwaters [*Meire et al.*, 2015]. Sampling stations where these negative RR fractions were observed also exhibit significant decreases in pCO_{2sw} in comparison to stations with positive RR fractions. The low pCO_{2sw} of these waters may be related to earlier phytoplankton blooms driven by increased nutrients from glaciers, or simply from the extremely low TA and DIC observed in glacial meltwaters [*Evans et al.*, 2014; *Meire et al.*, 2015].

5.3 Future Implications of Increased Freshwater

In this study we have found freshwater inputs to play a major role in the variation of pCO_{2sw} throughout the eastern Canadian Arctic. Significant SIM within the surface waters of eastern Baffin Bay were found to decrease pCO_{2sw} at the surface. This decrease was likely also supplemented by glacial melt inputs from western Greenland. Additionally, high fractions of river runoff were observed in the surface waters of Nares Strait, with the highest pCO_{2sw} in Kennedy Channel linked to the presence of ACW. As the climate of the Arctic region continues to change, so to will the contributions of these freshwater inputs to the surface ocean. River runoff has significantly increased in recent years [*Déry et al.*, 2009] along with increasing surface air temperatures throughout the Arctic region [*Serreze et al.*, 2009; *Serreze and Barry*, 2011]. Arctic rivers have been found to contain high concentrations of DIC and generally constitute heterotrophic environments, contributing to higher pCO_{2sw} within the rivers themselves [*Tank et al.*, 2012]. Therefore, with increasing riverine inputs to the surface ocean we can expect regions in proximity to large Arctic rivers to display increased pCO_{2sw}.

In this study we have also observed water masses originating outside the eastern Canadian Arctic to strongly influence surface pCO_{2sw} variations, such as the presence of ACW in Kennedy Channel. Woodgate et al. [2012] have found Pacific water inflow through the Bering Strait to have increased by ~50% from 2001 to 2011 (from ~0.7 Sv to ~1.1 Sv). Pacific waters are generally warmer, fresher, and contain more nutrients in comparison to Atlantic waters. Due to their high nutrient concentrations increases in Pacific water throughout the CAA may contribute to subsequent increases in overall primary production. However, based on our observations of

ACW in Kennedy Channel, increased ACW transport in particular may lead to more frequent areas of high pCO_{2sw}.

Sea ice models predict increased summer sea ice melt in the future, and that the Arctic Ocean may be completely ice-free in summer by 2020 [*Comiso and Parkinson*, 2004; *Overland and Wang*, 2013]. Although SIM does temporarily enhance the uptake of CO_2 within Arctic waters, it also contributes to strong stratification at the sea surface limiting nutrient availability for biological production. Both the studies of Cai et al. [2010] and Else et al. [2013b] provide evidence that this nutrient limitation in conjunction with higher sea surface temperatures will likely limit future summer CO_2 uptake in Arctic waters. Fransson et al. [2009] also speculated that nutrient limitation within surface waters of the CAA is responsible for low biological productivity despite an increase in available light throughout the ice-free season.

Overall, due to anticipated changes in freshwater inputs we speculate the waters of the eastern Canadian Arctic will enter a new summer state. Contributions from SIM will likely decrease in the future given the widespread expectation of thinner sea ice cover. This may lead to increases in pCO_{2sw} in eastern Baffin Bay where relatively warm and DIC-rich Atlantic waters are present. Contributions of glacial meltwater from the Greenland ice sheet will continue to influence this region, perhaps lowering pCO_{2sw} in specific areas and contributing significant nutrients to sustain summer phytoplankton blooms along the west coast of Greenland. Increased Pacific water and riverine inputs are anticipated to enter the channels of the CAA as far east as Nares Strait, and will likely enhance primary productivity due to their high nutrient concentrations. However, in areas influenced by enhanced riverine signals (such as ACW and outflows of major Arctic rivers)

this productivity may be limited due to high turbidity and CDOM concentrations preventing the penetration of light into surface waters. Enhanced river inputs will also produce a stable freshwater lens at the sea surface, preventing the vertical mixing of nutrients.

6.0 CONCLUSIONS

Continuous measurements of sea-surface pCO_{2sw} throughout the eastern Canadian Arctic reveal the waters of this region to be consistently undersaturated in CO_2 throughout the summer season. Therefore, the entire region has been shown to act as a summertime sink of atmospheric CO_2 with average uptake rates of -6.6 and -5.2 mmol C m^{-2} d^{-1} in 2013 and 2014 respectively. Coincident measurements of surface seawater temperature (T_{sw}) and salinity show the lowest recorded pCO_{2sw} measurements occurring in areas of both low T_{sw} and salinity, and were often linked to the presence of significant sea ice cover. The lowest pCO_{2sw} value recorded (144.8 μatm) was located just east of Devon Island, with another pocket of low pCO_{2sw} just south of the island. No sea ice cover was recorded in this area, and it is speculated that these low pCO_{2sw} values may be due to glacial ice melt from the Devon ice cap. Many other low pCO_{2sw} observations were made in proximity to glacial ice, such as within the Petermann Fjord in 2013 and along the west coast of Greenland in 2014. These areas all displayed low pCO_{2sw} values.

Measurements of $\delta^{18}O$ (2013) and TA (2014) collected at discrete sampling stations were utilized as freshwater tracers, allowing inputs of meteoric water (MW) or river runoff (RR) to be distinguished from contributions of sea ice melt (SIM). High concentrations of SIM were found in proximity to melting ice floes within Barrow Strait, and also throughout the surface mixed layer of eastern Baffin Bay. High positive SIM fractions in eastern Baffin Bay were found extending to depths of 100 m in the water column, indicating the advection of this SIM signal by

the West Greenland Current (WGC). The low DIC and TA of SIM is responsible for significantly lowering pCO_{2sw} within eastern Baffin Bay. Here our freshwater decomposition also revealed negative RR fractions at the surface, which are hypothesized to signal the presence of low TA glacial meltwaters originating from the west coast of Greenland. Overall, regions displaying high positive SIM fractions were found to coincide with very low measurements of pCO_{2sw}.

The highest fractions of MW and RR in both years were found within Petermann Fjord and Nares Strait, respectively. High MW fractions in Petermann Fjord likely signal the influence of glacial ice melt from the Petermann Glacier, and are found occurring with low pCO_{2sw}. Significant RR fractions within Kennedy Channel (northern Nares Strait) were found extending to depths of ~50 m, indicating the presence of a water mass carrying this riverine signal. Salinity and chemical characteristics of this water match with those of Alaskan Coastal Water (ACW), a summer Pacific water mass known to display a strong riverine signal mainly from the Yukon river [*Steele et al.*, 2004]. ACW has been observed to travel as far east as the Lincoln Sea north of Ellesmere Island, transported by the North American boundary current [*Newton and Sotirin*, 1997]. Our highest recorded measurements of pCO_{2sw} in 2014 coincide with the location of this ACW. Further south in Nares Strait positive fractions of RR are still observed, but are confined to the top ~20 m of the water column. This RR signal may also be related to the presence of ACW, or may be local contributions from the smaller rivers and glacial streams of Greenland or Ellesmere Island.

Biology was found to play a more minor role in summer, with low chlorophyll-*a* concentrations ubiquitous throughout the surface waters of the region. This is quite common within the Arctic Ocean, as the initial spring phytoplankton bloom depletes surface waters of their nutrients, followed by large freshwater inputs throughout the summer which strongly stratify the surface layer preventing the upward mixing of nutrients from below [*Tremblay et al.*, 2008]. The only exception to this was located in Petermann Fjord, where it is hypothesized that glacial runoff contributes nutrients to the surface waters sustaining a large phytoplankton bloom. Despite low productivity at the surface, significant subsurface chlorophyll-a maxima (SCMs) were observed in certain locations. However, it is unlikely these SCMs would affect rates of air-sea CO_2 exchange as strong stratification of the surface layer prevents vertical mixing.

Based on the results of this investigation and future predictions of an ice-free Arctic Ocean in summer [*Overland and Wang*, 2013], we expect the surface waters within eastern Baffin Bay will likely display higher pCO_{2sw} in the future than presently observed. However, substantial inputs of glacial ice melt from the western coast of Greenland will likely lower pCO_{2sw} in small areas of this region. It is also likely that increased Pacific water inflow [*Woodgate et al.*, 2012] will substantially impact rates of primary production throughout the CAA, however it is difficult to predict the exact consequences of this. Increased riverine inputs from large rivers such as the Mackenzie and Yukon rivers will continue to create large runoff plumes in the surface ocean, exhibiting high DIC (and potentially CDOM), contributing to sustained areas of high pCO_{2sw} in the future.

Throughout this investigation we have speculated much about the influence of glacial ice melt on pCO_{2sw}. Future investigations would benefit from additional research into the carbonate chemistry of glacial ice melt, and the identification of chemical tracers capable of determining the spatial extent of this freshwater source in the surface ocean. Further research into nutrient dynamics within the eastern Canadian Arctic are also recommended, especially in light of increasing Pacific inflows to the Arctic Ocean [*Woodgate et al.*, 2012]. It is expected that increases in nutrient-rich Pacific waters would lead to increased primary production within the Arctic Ocean, however significant freshwater inputs may continue to cause strong stratification at the surface, perhaps leading to stronger and more extensive SCMs. The continuation of underway pCO_{2sw} measurements throughout this region is also of importance, as it would lead to increased understanding of the seasonal and inter-annual variability of pCO_{2sw} and air-sea CO_2 fluxes.

REFERENCES

Alkire, M. B., K. K. Falkner, T. Boyd, and R. W. Macdonald (2010), Sea ice melt and meteoric water distributions in Nares Strait, Baffin Bay, and the Canadian Arctic Archipelago, *J. Mar. Res.*, *68*(6), 767–798.

Alkire, M. B., J. Morison, and R. Andersen (2015), Variability in the meteoric water, sea-ice melt, and Pacific water contributions to the central Arctic Ocean, 2000-2014, *J. Geophys. Res. Ocean.*, *120*, 1573–1598, doi:10.1002/2014JC010023.

Anderson, L. G., S. Jutterström, S. Kaltin, E. P. Jones, and G. Bjork (2004), Variability in river runoff distribution in the Eurasian Basin of the Arctic Ocean, *J. Geophys. Res.*, *109*(C1), 1–8, doi:10.1029/2003JC001773.

Ardyna, M., M. Babin, M. Gosselin, E. Devred, S. Bélanger, a. Matsuoka, and J. E. Tremblay (2013), Parameterization of vertical chlorophyll a in the Arctic Ocean: Impact of the subsurface chlorophyll maximum on regional, seasonal, and annual primary production estimates, *Biogeosciences*, *10*(6), 4383–4404, doi:10.5194/bg-10-4383-2013.

Arrhenius, S. (1896), On the influence of carbonic acid in the air upon the temperature of the ground, *Philos. Mag. J. Sci.*, *41*, 237–376.

Arrigo, K. R., and C. W. Brown (1996), Impact of chromophoric dissolved organic matter on UV inhibition of primary productivity in the sea, *Mar. Ecol. Prog. Ser.*, *140*(1-3), 207–216, doi:10.3354/meps140207.

Azetsu-Scott, K., B. Petrie, P. Yeats, and C. Lee (2012), Composition and fluxes of freshwater through Davis Strait using multiple chemical tracers, *J. Geophys. Res.*, *117*(C12), C12011, doi:10.1029/2012JC008172.

Bâcle, J., E. C. Carmack, and R. G. Ingram (2002), Water column structure and circulation under the North Water during spring transition: April-July 1998, *Deep. Res. Part II*, *49*(22-23), 4907–4925, doi:10.1016/S0967-0645(02)00170-4.

Bamber, J., M. Van Den Broeke, J. Ettema, J. Lenaerts, and E. Rignot (2012), Recent large increases in freshwater fluxes from Greenland into the North Atlantic, *Geophys. Res. Lett.*, *39*(19), 8–11, doi:10.1029/2012GL052552.

Barber, D. G., and R. a. Massom (2007), The Role of Sea Ice in Arctic and Antarctic Polynyas, in *Polynyas: Windows to the World*, vol. 74, edited by W. O. Smith and D. G. Barber, pp. 1–54, Elsevier.

Bates, N., and J. Mathis (2009), The Arctic Ocean marine carbon cycle: evaluation of air-sea CO2 exchanges, ocean acidification impacts and potential feedbacks, *Biogeosciences*, *6*, 2433–2459.

Bédard, P., C. Hillaire-Marcel, and P. Pagé (1981), 18O modelling of freshwater inputs in Baffin Bay and Canadian Arctic coastal waters, *Nature*, *293*(5830), 287–289, doi:10.1038/293287a0.

Bhatia, M. P., E. B. Kujawinski, S. B. Das, C. F. Breier, P. B. Henderson, and M. A. Charette (2013), Greenland meltwater as a significant and potentially bioavailable source of iron to the ocean, *Nat. Geosci.*, *6*(4), 274–278, doi:10.1038/ngeo1746.

Cai, W.-J. et al. (2010), Decrease in the CO2 uptake capacity in an ice-free Arctic Ocean basin, *Science (80-.).*, *329*(5991), 556–559, doi:10.1126/science.1189338.

Carmack, E. C., R. W. Macdonald, and S. Jasper (2004), Phytoplankton productivity on the Canadian Shelf of the Beaufort Sea, *Mar. Ecol. Prog. Ser.*, *277*, 37–50, doi:10.3354/meps277037.

Clarke, R. A. (1984), Transports through the Cape Farewell-Flemish Cap section, *Rapp. P.- v. Reun. Cons. Int Explor. Mer*, *185*, 120–130.

Comiso, J., and C. Parkinson (2004), Satellite-observed changes in the Arctic, *Phys. Today*, *57*(8), 38–44, doi:10.1063/1.1801866.

Cross, J., J. Mathis, K. Frey, C. Cosca, S. Danielson, N. Bates, R. Feely, T. Takahashi, and W. Evans (2014), Annual sea-air CO2 fluxes in the Bering Sea: Insights from new autumn and winter observations of a seasonally ice-covered continental shelf, *J. Geophys. Res. Ocean.*, *119*, 6693–6708, doi:10.1002/2013JC009579.

Déry, S. J., M. A. Hernández-Henríquez, J. E. Burford, and E. F. Wood (2009), Observational evidence of an intensifying hydrological cycle in northern Canada, *Geophys. Res. Lett.*, *36*(13), 1–5, doi:10.1029/2009GL038852.

Dickson, A. G., C. L. Sabine, and J. R. Christian (2007), Guide to best practices for ocean CO2 measurements., *PICES Spec. Publ.*, *3*, p191, doi:10.1159/000331784.

Ekwurzel, B., P. Schlosser, R. A. Mortlock, R. G. Fairbanks, and J. H. Swift (2001), River runoff, sea ice meltwater, and Pacific water distribution and mean residence times in the Arctic Ocean, *J. Geophys. Res.*, *106*(C5), 9075, doi:10.1029/1999JC000024.

Else, B. G. T., T. N. Papakyriakou, M. A. Granskog, and J. J. Yackel (2008), Observations of sea surface fCO2 distributions and estimated air-sea CO2 fluxes in the Hudson Bay region (Canada) during the open water season, *J. Geophys. Res.*, *113*(C8), C08026, doi:10.1029/2007JC004389.

Else, B. G. T., T. N. Papakyriakou, M. G. Asplin, D. G. Barber, R. J. Galley, L. A. Miller, and A. Mucci (2013a), Annual cycle of air-sea CO2 exchange in an Arctic Polynya Region, *Global Biogeochem. Cycles*, *27*(2), 388–398, doi:10.1002/gbc.20016.

Else, B. G. T., R. J. G. B. Lansard, D. G. Barber, K. Brown, L. a Miller, A. Mucci, T. N. Papakyriakou, J. É. Tremblay, and S. Rysgaard (2013b), Further observations of a decreasing atmospheric CO2 uptake capacity in the Canada Basin (Arctic Ocean) due to sea ice loss, *Geophys. Res. Lett.*, *40*(6), 1132–1137, doi:10.1002/grl.50268.

Evans, W., J. T. Mathis, and J. N. Cross (2014), Calcium carbonate corrosivity in an Alaskan inland sea, *Biogeosciences*, *11*(2), 365–379, doi:10.5194/bg-11-365-2014.

Evans, W. et al. (2015), Sea-air CO2 exchange in the western Arctic coastal ocean, *Global Biogeochem. Cycles*, 1–20, doi:10.1002/2015GB005153.

Fairbanks, R. (1982), The Origin of Continental Shelf and Slope Water in the New York Bight and Gulf of Maine: Evidence from H218O/ H216O Ratio Measurements, *J. Geophys. Res.*, *87*(C8), 5796–5808.

Fransson, A., M. Chierici, and Y. Nojiri (2009), New insights into the spatial variability of the surface water carbon dioxide in varying sea ice conditions in the Arctic Ocean, *Cont. Shelf Res.*, *29*(10), 1317–1328, doi:10.1016/j.csr.2009.03.008.

Frew, N. M. (1997), The role of organic films in air–sea gas exchange, in *The Sea Surface and Global Change*, pp. 121–172.

Frew, N. M. (2004), Air-sea gas transfer: Its dependence on wind stress, small-scale roughness, and surface films, *J. Geophys. Res.*, *109*(C8), 1–23, doi:10.1029/2003JC002131.

Hamilton, E. I. (1984), A manual of chemical & biological methods for seawater analysis, *Mar. Pollut. Bull.*, *15*(11), 419–420, doi:10.1016/0025-326X(84)90262-5.

Hamilton, J., and Y. Wu (2013), Synopsis and trends in the physical environment of Baffin Bay and Davis Strait, *Can. Tech. Rep. Hydrogr. Ocean Sci.*, *282*, 1–39.

Ho, D. T., C. S. Law, M. J. Smith, P. Schlosser, M. Harvey, and P. Hill (2006), Measurements of air-sea gas exchange at high wind speeds in the Southern Ocean: Implications for global parameterizations, *Geophys. Res. Lett.*, *33*(16), 1–6, doi:10.1029/2006GL026817.

Hopkins, T. S. (1991), The GIN Sea—A synthesis of its physical oceanography and literature review 1972–1985, *Earth-Science Rev.*, *30*(3-4), 175–318, doi:10.1016/0012-8252(91)90001-V.

Ito, H. (1982), Wind through a channel - surface wind measurements in Smith Sound and Jones Sound in Northern Baffin Bay, *J. Appl. Meteorol.*, *21*(8), 1053–1062.

Jähne, B., G. Heinz, and W. Dietrich (1987), Measurement of the diffusion coefficients of sparingly soluble gases in water, *J. Geophys. ...*, *92*.

Johnson, H. L., a. Münchow, K. K. Falkner, and H. Melling (2011), Ocean circulation and properties in Petermann Fjord, Greenland, *J. Geophys. Res. Ocean.*, *116*(1), 1–18, doi:10.1029/2010JC006519.

Liss, P. S., and L. Merlivat (1986), Air–Sea Gas Exchange Rates: Introduction and Synthesis, in *The Role of Air–Sea Exchange in Geochemical Cycles*, edited by P. Buat-Menard, pp. 113–127, D. Reidel, Norwell, MA.

Macdonald, R. W., D. W. Paten, E. C. Carmack, and A. Omstedt (1995), The freshwater budget and under-ice spreading of Mackenzie River water in the Canadian Beaufort Sea based on salinity and 18O/16O measurements in water and ice, *J. Geophys. Res.*, *100*, 895–919.

MacIntyre, S., R. Wanninkhof, and J. P. Chanton (1995), Trace gas exchange across the air-water interface in freshwatre and coastal marine environments, in *Biogenic Trace Gases: Measuring emissions from Soil and Water*, edited by P. A. Matson and R. C. Hariss, pp. 52–97, Blackwell Science Ltd., Oxford.

Majoube, M. (1971), Fractionnement en oxygene-18 et en deuterium entre l'eau et sa vapeur, *J. Chim. Phys.*, *58*, 1423–1436.

McGillis, W. R., J. B. Edson, J. E. Hare, and C. W. Fairall (2001), Direct covariance air-sea CO2 fluxes, *J. Geophys. Res.*, *106*(C8), 16729–16745, doi:10.1029/2000JC000506.

McGillis, W. R. et al. (2004), Air-sea CO2 exchange in the equatorial Pacific, *J. Geophys. Res. C Ocean.*, *109*(8), 1–17, doi:10.1029/2003JC002256.

McLaughlin, F. A., E. C. Carmack, R. G. Ingram, W. J. Williams, and C. Michel (2004), Oceanography of the Northwest Passage, in *The Sea*, vol. 14, edited by A. R. Robinson and K. . Brink, pp. 1211–1242, Harvard University Press.

Meire, L., D. H. Søgaard, J. Mortensen, F. J. R. Meysman, K. Soetaert, K. E. Arendt, T. Juul-Pedersen, M. E. Blicher, and S. Rysgaard (2015), Glacial meltwater and primary production are drivers of strong CO2 uptake in fjord and coastal waters adjacent to the Greenland Ice Sheet, *Biogeosciences*, *12*(8), 2347–2363, doi:10.5194/bg-12-2347-2015.

Melling, H., Y. Gratton, and G. Ingram (2010), Ocean circulation within the North Water polynya of Baffin Bay, *Atmosphere-Ocean*, *39*(3), 301–325, doi:10.1080/07055900.2001.9649683.

Miller, L. A. et al. (2002), Carbon distributions and fluxes in the North Water, 1998 and 1999, *Deep. Res. Part II Top. Stud. Oceanogr.*, *49*(22-23), 5151–5170.

Miller, L. A., G. Carnat, B. G. T. Else, N. Sutherland, and T. N. Papakyriakou (2011), Carbonate system evolution at the Arctic Ocean surface during autumn freeze-up, *J. Geophys. Res.*, *116*, C00G04, doi:10.1029/2011JC007143.

Mucci, A., B. Lansard, L. A. Miller, and T. N. Papakyriakou (2010), CO2 fluxes across the air-sea interface in the southeastern Beaufort Sea: Ice-free period, *J. Geophys. Res. Ocean.*, *115*(4), 1–14, doi:10.1029/2009JC005330.

Mundy, C. J., and D. G. Barber (2001), On the relationship between spatial patterns of sea–ice type and the mechanisms which create and maintain the North Water (NOW) polynya, *Atmosphere-Ocean*, *39*(3), 327–341, doi:10.1080/07055900.2001.9649684.

Newton, J. L., and B. J. Sotirin (1997), Boundary undercurrent and water mass changes in the Lincoln Sea, *J. Geophys. Res.*, *102*(C2), 3393, doi:10.1029/96JC03441.

Nightingale, P. D., G. Malin, C. S. Law, A. J. Watson, P. S. Liss, M. I. Liddicoat, J. Boutin, and R. C. Upstill-Goddard (2000), In situ evaluation of air-sea gas exchange parameterizations using novel conservative and volatile tracers, *Global Biogeochem. Cycles*, *14*(1), 373, doi:10.1029/1999GB900091.

Östlund, H. G., and G. Hut (1984), Arctic Ocean water mass balance from isotope data, *J. Geophys. Res. Ocean.*, *89*(C4), 6373–6381, doi:10.1029/JC089iC04p06373.

Overland, J. E., and M. Wang (2013), When will the summer Arctic be nearly sea ice free?, *Geophys. Res. Lett.*, *40*(10), 2097–2101, doi:10.1002/grl.50316.

Pierrot, D., C. Neill, K. Sullivan, R. Castle, R. Wanninkhof, H. Lüger, T. Johannessen, A. Olsen, R. A. Feely, and C. E. Cosca (2009), Recommendations for autonomous underway pCO2 measuring systems and data-reduction routines, *Deep. Res. Part II*, *56*(8-10), 512–522, doi:10.1016/j.dsr2.2008.12.005.

Le Quéré, C., T. Takahashi, E. T. Buitenhuis, C. Rödenbeck, and S. C. Sutherland (2010), Impact of climate change and variability on the global oceanic sink of CO2, *Global Biogeochem. Cycles*, *24*(GB4007), doi:10.1029/2009GB003599.

Redfield, A. C., B. H. Ketchum, and F. A. Richards (1963), The Influence of Organisms on the Composition of Sea-water, in *The Sea*, edited by M. Hill, pp. 26–77, Wiley Interscience, New York.

Reeh, N., H. Oerter, and H. H. Thomsen (2002), Comparison between Greenland ice-margin and ice-core oxygen-18 records, *Ann. Glaciol.*, *35*(1), 136–144, doi:10.3189/172756402781817365.

Rignot, E., I. Velicogna, M. R. Van Den Broeke, A. Monaghan, and J. Lenaerts (2011), Acceleration of the contribution of the Greenland and Antarctic ice sheets to sea level rise, *Geophys. Res. Lett.*, *38*, 1–5, doi:10.1029/2011GL046583.

Rysgaard, S., R. N. Glud, M. K. Sejr, J. Bendtsen, and P. B. Christensen (2007), Inorganic carbon transport during sea ice growth and decay: A carbon pump in polar seas, *J. Geophys. Res.*, *112*(C3), C03016, doi:10.1029/2006JC003572.

Rysgaard, S., J. Mortensen, T. Juul-Pedersen, L. L. Sørensen, K. Lennert, D. H. Søgaard, K. E. Arendt, M. E. Blicher, M. K. Sejr, and J. Bendtsen (2012), High air–sea CO2 uptake rates in nearshore and shelf areas of Southern Greenland: Temporal and spatial variability, *Mar. Chem.*, *128-129*, 26–33, doi:10.1016/j.marchem.2011.11.002.

Sarmiento, J. L., and N. Gruber (2006), Carbon Cycle, in *Ocean Biogeochemical Dynamics*, pp. 318–349, Princeton University Press, Princeton.

Schlosser, P., and R. Newton (2002), Decrease of river runoff in the upper waters of the Eurasian Basin, Arctic Ocean, between 1991 and 1996: Evidence from δ18O data, *Geophys. Res. Lett.*, *29*(9), 2–5, doi:10.1029/2001gl013135.

Sejr, M. K., D. Krause-Jensen, S. Rysgaard, L. L. Sørensen, P. B. Christensen, and R. N. Glud (2011), Air-sea flux of CO2 in arctic coastal waters influenced by glacial melt water and sea ice, *Tellus B*, *63*(5), 815–822, doi:10.1111/j.1600-0889.2011.00540.x.

Serreze, M. C., and R. G. Barry (2011), Processes and impacts of Arctic amplification: A research synthesis, *Glob. Planet. Change*, *77*(1-2), 85–96, doi:10.1016/j.gloplacha.2011.03.004.

Serreze, M. C., A. P. Barrett, J. C. Stroeve, D. N. Kindig, and M. M. Holland (2009), The emergence of surface-based Arctic amplification, *Cryosph.*, *3*, 11–19.

Sharp, M., D. O. Burgess, J. G. Cogley, M. Ecclestone, C. Labine, and G. J. Wolken (2011), Extreme melt on Canada's Arctic ice caps in the 21st century, *Geophys. Res. Lett.*, *38*(11), 3–7, doi:10.1029/2011GL047381.

Shiklomanov, I. A. (2000), Appraisal and Assessment of World Water Resources, *Water Int.*, *25*(1), 11–32, doi:10.1080/02508060008686794.

Smith, S. D., R. D. Muench, and C. H. Pease (1990), Polynyas and leads: An overview of physical processes and environment, *J. Geophys. Res.*, *95*(C6), 9461, doi:10.1029/JC095iC06p09461.

Spreen, G., S. Kern, D. Stammer, and E. Hansen (2009), Fram Strait sea ice volume export estimated between 2003 and 2008 from satellite data, *Geophys. Res. Lett.*, *36*(19), 1–6, doi:10.1029/2009GL039591.

Steele, M., J. Morison, W. Ermold, I. Rigor, and M. Ortmeyer (2004), Circulation of summer Pacific halocline water in the Arctic Ocean, *J. Geophys. Res.*, *109*(C2), 1–18, doi:10.1029/2003JC002009.

de Steur, L., E. Hansen, R. Gerdes, M. Karcher, E. Fahrbach, and J. Holfort (2009), Freshwater fluxes in the East Greenland Current: A decade of observations, *Geophys. Res. Lett.*, *36*(23), L23611, doi:10.1029/2009gl041278.

Stirling, I. (1980), The Biological Importance of Polynyas in the Canadian Arctic, *Arctic*, *33*(2), 303–315.

Stroeve, J., M. M. Holland, W. Meier, T. Scambos, and M. Serreze (2007), Arctic sea ice decline: Faster than forecast, *Geophys. Res. Lett.*, *34*(9), 1–5, doi:10.1029/2007GL029703.

Stull, R. B. (1988), An Introduction to Boundary Layer Meteorology, *Book*, *13*, 666, doi:10.1007/978-94-009-3027-8.

Sutherland, D. A., and R. S. Pickart (2008), The East Greenland Coastal Current: Structure, variability, and forcing, *Prog. Oceanogr.*, *78*(1), 58–77, doi:10.1016/j.pocean.2007.09.006.

Sweeney, C., E. Gloor, A. R. Jacobson, R. M. Key, G. McKinley, J. L. Sarmiento, and R. Wanninkhof (2007), Constraining global air-sea gas exchange for CO2 with recent bomb 14C measurements, *Global Biogeochem. Cycles*, *21*(2), 1–10, doi:10.1029/2006GB002784.

Takahashi, T., J. Olafsson, J. G. Goddard, D. W. Chipman, and S. C. Sutherland (1993), and nutrients in the high-latitude surface oceans: A comparative study, *Global Biogeochem. Cycles*, *7*(4), 843, doi:10.1029/93GB02263.

Tan, F., and P. Strain (1980), The distribution of sea ice meltwater in the eastern Canadian Arctic, *J. Geophys. Res.*, *85*(C4), 1925–1932, doi:10.1029/JC085iC04p01925.

Tang, C. C. L., C. K. Ross, T. Yao, B. Petrie, B. M. DeTracey, and E. Dunlap (2004), The circulation, water masses and sea-ice of Baffin Bay, *Prog. Oceanogr.*, *63*, 183–228, doi:10.1016/j.pocean.2004.09.005.

Tank, S. E., P. A. Raymond, R. G. Striegl, J. W. McClelland, R. M. Holmes, G. J. Fiske, and B. J. Peterson (2012), A land-to-ocean perspective on the magnitude, source and implication of DIC flux from major Arctic rivers to the Arctic Ocean, *Global Biogeochem. Cycles*, *26*(4), 1–15, doi:10.1029/2011GB004192.

Tremblay, J. É., K. Simpson, J. Martin, L. Miller, Y. Gratton, D. Barber, and N. M. Price (2008), Vertical stability and the annual dynamics of nutrients and chlorophyll fluorescence in the coastal, southeast Beaufort Sea, *J. Geophys. Res. Ocean.*, *113*(7), 1–14, doi:10.1029/2007JC004547.

Tremblay, J.-É., Y. Gratton, E. C. Carmack, C. D. Payne, and N. M. Price (2002), Impact of the large‐scale Arctic circulation and the North Water Polynya on nutrient inventories in Baffin Bay, *J. Geophys. Res.*, *107*(C8), 1–15, doi:10.1029/2000JC000595.

Wanninkhof, R. (1992), Relationship Between Wind Speed and Gas Exchange, *J. Geophys. Res.*, *97*(92), 7373–7382, doi:10.1029/92JC00188.

Wanninkhof, R. (2014), Relationship between wind speed and gas exchange over the ocean revisited, *Limnol. Oceanogr. Methods*, *12*, 351–362, doi:10.1029/92JC00188.

Wanninkhof, R., and W. R. McGillis (1999), A cubic relationship between air‐sea CO2 exchange and wind speed, *Geophys. Res. Lett.*, *26*(13), 1889–1892, doi:10.1029/1999GL900363.

Wanninkhof, R., W. E. Asher, D. T. Ho, C. Sweeney, and W. R. McGillis (2009), Advances in quantifying air-sea gas exchange and environmental forcing., *Ann. Rev. Mar. Sci.*, *1*, 213–244, doi:10.1146/annurev.marine.010908.163742.

Weiss, R. F. (1974), Carbon dioxide in water and seawater: the solubility of a non-ideal gas, *Mar. Chem.*, *2*(3), 203–215, doi:10.1016/0304-4203(74)90015-2.

Wilson, K. J., D. G. Barber, and D. J. King (2001), Validation and production of RADARSAT‐1 derived ice‐motion maps in the North Water (NOW) polynya, January ‐ December 1998, *Atmosphere-Ocean*, *39*(3), 257–278, doi:10.1080/07055900.2001.9649680.

Woodgate, R. A., T. J. Weingartner, and R. Lindsay (2012), Observed increases in Bering Strait oceanic fluxes from the Pacific to the Arctic from 2001 to 2011 and their impacts on the Arctic Ocean water column, *Geophys. Res. Lett.*, *39*, 2–7, doi:10.1029/2012GL054092.

Woolf, D. K. (2005), Parametrization of gas transfer velocities and sea-state-dependent wave breaking, *Tellus, Ser. B Chem. Phys. Meteorol.*, *57*(2), 87–94, doi:10.1111/j.1600-0889.2005.00139.

Yamamoto-Kawai, M., N. Tanaka, and S. Pivovarov (2005), Freshwater and brine behaviors in the Arctic ocean deduced from historical data of δ18O and alkalinity (1929-2002 A.D.), *J. Geophys. Res. Ocean.*, *110*, 1–16, doi:10.1029/2004JC002793.

Zappa, C. J., W. E. Asher, A. T. Jessup, J. Klinke, and S. R. Long (2004), Microbreaking and the enhancement of air-water transfer velocity, *J. Geophys. Res. C Ocean.*, *109*(8), 1–18, doi:10.1029/2003JC001897.

Zappa, C. J., W. R. McGillis, P. A. Raymond, J. B. Edson, E. J. Hintsa, H. J. Zemmelink, J. W. H. Dacey, and D. T. Ho (2007), Environmental turbulent mixing controls on air-water gas exchange in marine and aquatic systems, *Geophys. Res. Lett.*, *34*(10), 1–6, doi:10.1029/2006GL028790.

Zappa, C. J., D. T. Ho, W. R. McGillis, M. L. Banner, J. W. H. Dacey, L. F. Bliven, B. Ma, and J. Nystuen (2009), Rain-induced turbulence and air-sea gas transfer, *J. Geophys. Res. Ocean.*, *114*(7), 1–17, doi:10.1029/2008JC005008.

Zeebe, R. E., and D. A. Wolf-Gladrow (2001), *CO2 in seawater: equilibrium, kinetics, isotopes*, Elsevier.PDF Thesi